Construction and Building Materials 439 (2024) 137276

Contents lists available at ScienceDirect

Construction and Building Materials

journal homepage: www.elsevier.com/locate/conbuildmat

Experimental and deep neural network approaches on strength evaluation of ternary blended concrete

Solomon Oyebisi [a,b,*], Thamer Alomayri [c]

[a] Department of Civil Engineering, Covenant University, Ota, Nigeria
[b] Department of Civil Engineering, The University of the South Pacific, Suva, Fiji
[c] Department of Physics, Faculty of Science, Umm Al-Qura University, 21955, Makkah, Saudi Arabia

ARTICLE INFO

Keywords:
Ash
Cement
Compressive strength
Deep neural network
Recycling
Ternary blended concrete

ABSTRACT

The manufacture of cement contributes significantly to carbon dioxide emissions; hence, the building and construction industry has focused on environmentally friendly cement substitutes. Supplementary cementitious materials (SCMs) such as calcite powder (CP) and Vitellaria paradoxa ash (VPA) offers sustainable substitutes. Thus, this study calcined shea nutshell at 700 °C for 3 h, obtaining VPA. Portland limestone cement was partially replaced by calcite powder and VPA at 5–15 wt% to produce 25 and 30 MPa concrete grades. Split tensile strength (STS), flexural strength (FS), and compressive strength (CS) of TBC samples were tested after 3–120 days of curing. Deep neural network (DNN) models, having 3 hidden layers with 5–30 nodes, were engaged to predict the strengths with respect to the concrete mix design proportions. For each strength, 108 datasets were obtained from the experimental data. Out of these values, 100 datasets were utilized to train the models, and the remaining 8 values were used to confirm the model's accuracy. The results revealed an improvement in concrete's CS, FS, and STS at 10 % VPA and 10 % CP replacements. The 7–25–25–25-1 network topologies demonstrated robust correlation for training, validating, and testing the input and output variables of CS and FS with correlation coefficients (R) of 99.92 and 99.01 % compared to other architectures. However, 7-20–20–20-1 network structure exhibited the best performance metric for predicting the STS of TBC with 99.51 % R. Strong relationships were found between the created model's validity and the raw experimental datasets, with R^2 values for CS, FS, and STS yielding 98.45, 99.75, and 99.35 %. By using this technique, TBC incorporating SCMs would be of higher quality.

1. Introduction

Concrete is ideal for construction and building, particularly in our ever-changing infrastructural systems. Concrete's significance will continue to grow as new applications and ecologically friendly technology are found [1]. By 2050, it is projected that more than 18 billion tons of concrete will be required yearly [2]. Still, the manufacture of Portland cement (PC), which is required to make concrete, is usually attributed to the main source of CO_2 emissions in the atmosphere. PC production accounts for 2–3 % of global energy consumption, whereas the use of concrete contributes significantly to greenhouse gas emissions, accounting for 5–8 % of global emissions. [3]. Therefore, environmentally friendly substitute materials are recycled for use as building and construction materials. For instance, using rice straw ash and nano eggshell powder as cement substitutes improves the mechanical properties, durability, and dry shrinkage of concrete [4]. The replacement of cement with 1.2 % of nano titanium and 20 % of fly ash reduced the workability and improved the mechanical properties of ultra-high performance concrete [5]. Concrete made with 15 wt% Vitellaria paradoxa ash (VPA) or shea nutshell ash exhibited lower economic cost, a higher sustainability score, and less embodied energy and carbon dioxide than conventional concrete [6]. A 2 wt% VPA and 4 wt% PC are suitable for use as stabilizers in earth blocks [7]. The inclusion of 15 wt% kaolin clay and 30 wt% shea nutshell particles in lieu

Abbreviation: PLC, Portland limestone cement; VPA, Vitellaria paradoxa ash; CP, Calcite powder; FA, Fine aggregate; CA, Coarse aggregate; BA, Binder-aggregate ratio; WB, Water-binder ratio; CD, Curing day; CS, Compressive strength; FS, Flexural strength; STS, Split tensile strength; DNN, Deep neural networks; LM, Levenberg Marquardt; ML, Machine learning; SCMs, Supplementary cementitious materials; TBC, Ternary blended concrete.

* Corresponding author at: Department of Civil Engineering, Covenant University, Ota, Nigeria.
E-mail addresses: sotech281.ola@gmail.com (S. Oyebisi), tsomayri@uqu.edu.sa (T. Alomayri).

https://doi.org/10.1016/j.conbuildmat.2024.137276
Received 28 April 2024; Received in revised form 12 June 2024; Accepted 26 June 2024

Fig. 1. Binding materials used (a) PLC, (b) Shea nutshells, (c) VPA, and (d) CP.

Table 1
Constituents' physical properties.

Material	SG	BD (kg/m^3)	Water absorption (%)	Moisture content (%)
PLC	3.15	1440	-	-
CP	2.78	1125	-	-
VPA	2.45	998	-	-
FA	2.60	1620	0.30	0.70
CA	2.66	1650	0.20	0.80

Table 2
Oxide compositions.

Oxide content (%)	PLC	VPA	CP
CaO	64.90	6.62	97.15
SiO_2	21.60	54.85	0.18
Al_2O_3	5.85	18.78	0.02
Fe_2O_3	2.78	8.10	0.01
MgO	1.42	1.26	0.20
Na_2O	0.14	0.75	-
K_2O	0.19	1.85	-
SO_3	2.03	1.15	-
P_2O_5	-	0.25	-
Ti_2O	-	1.38	-
LOI @ 800°C	1.38	3.75	0.26

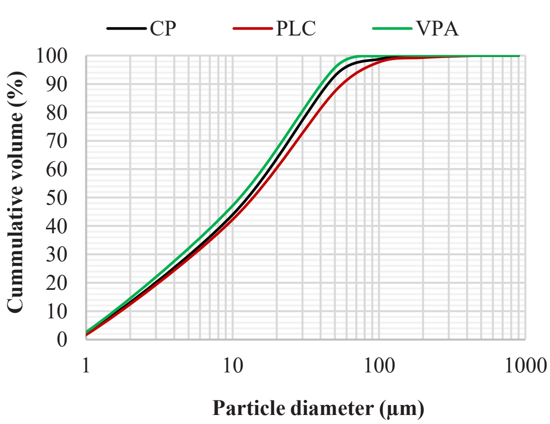

Fig. 2. PSD of binders.

of PC and fine aggregates improved the concrete's physical characteristics, strength, and durability [8]. Numerous characterization tests depicted shea nutshells as appropriate materials that can be recycled to enhance the economics of clay brick production [9]. Due to filler and nucleation mechanisms, replacing cement with 0–8 wt% [10] and 0–20 wt% [11] of calcite powder (CP) boosts the concrete's compressive strength (CS) and decreases its chloride permeability. However, because of the diluting effect, the CS of concrete decreased as the CP concentration increased from 0 to 35 wt% [12]. Adding CP to concrete at a

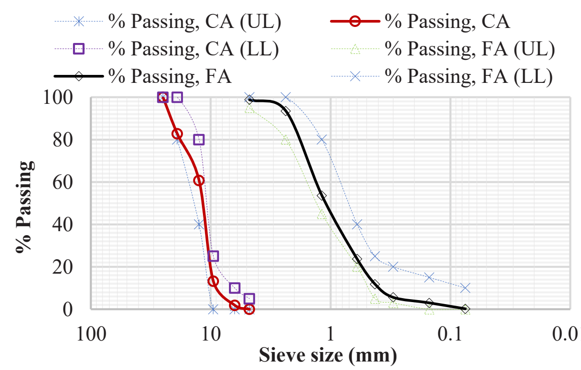

Fig. 3. Aggregates' PSD.

Table 3
Design proportions of the concrete samples (kg/m^3).

Grade	Constituents	VC0	VC5	VC10	VC15
C 25	PLC	326	293	261	228
	VPA	0	16.50	32.50	49
	CP	0	16.50	32.50	49
	FA	862	858	853	848
	CA	919	919	919	919
	Water	199	199	190	199
	W/B ratio	0.61	0.61	0.61	0.61
C 30	PLC	369	332	295	258
	VPA	0	18.50	37	55.50
	CP	0	18.50	37	55.50
	FA	828	822	815	808
	CA	919	919	919	919
	Water	199	199	199	199
	W/B ratio	0.54	0.54	0.54	0.54

weight proportion of 10–15 % is ideal for strengthening it [13,14]. Replacing cement with wheat straw ash significantly reduces concrete's drying shrinkage whereas substituting fine aggregates with glass particles enhances the concrete's compressive strength at elevated temperatures (up to 200 °C) [15]. The replacement of cement with 20 % sugarcane leaf ash or granite showed the best mechanical characteristics of the ultra-high performance concrete by 12.16 and 8.44 % increment [16].

Concrete is the primary building material used for structural components in modern architecture and construction. A structure must have the proper mechanical properties, such as CS, FS, and STS, in order to be sturdy and stable. Constructability and durability are considered throughout the design phase, which determines the percentage of varied components in concrete and necessitates multiple trials to determine the perfect combinations in order to meet the structural performance requirements [17]. This approach has economic and material losses due to rises in the required number of tests with the number of parameters and necessary performance [18–20].

Through the use of computational tools to reduce labour and time

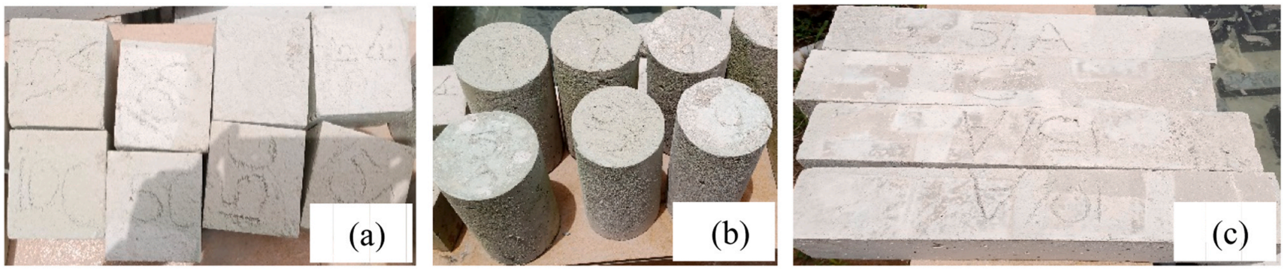

Fig. 4. Concrete samples for (a) cubes (100 mm × 100 mm × 100 mm), (b) cylinders (200 mm high ×100 mm diameter), and (c) beams (A 500 mm × 100 mm × 100 mm).

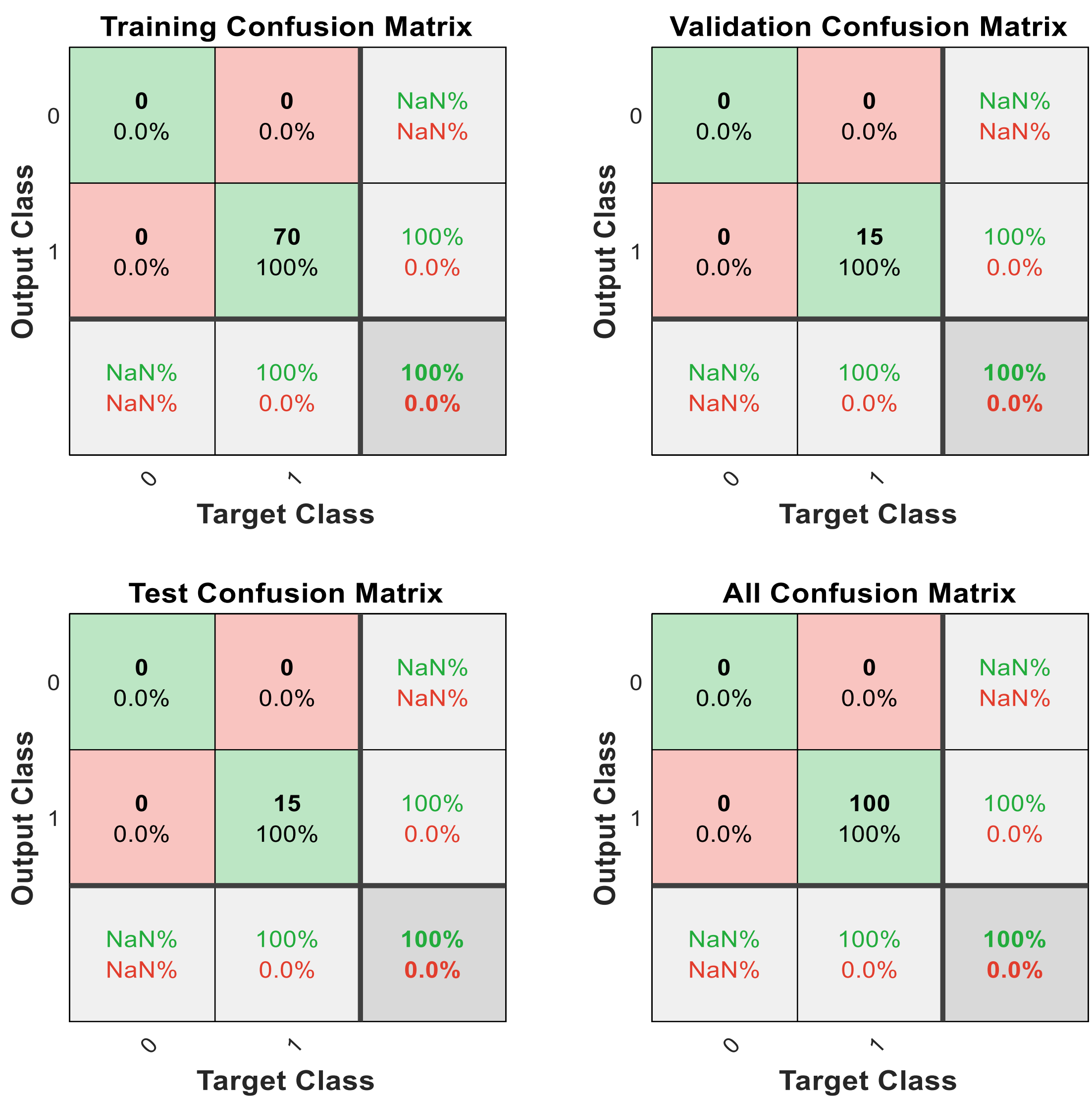

Fig. 5. Random division of datasets.

requirements, research has focused on supporting formulation design by studying the relationship between necessary performance, such as concrete's CS, and the quantities of ingredients employed [21–23]. The compositional percentage of constituents and concrete's necessary performance have been studied using mathematical formulas and empirical regression techniques [24,25]. The limitations of the input range or the constant need to predict the correlation between the parameters of the input and output make these techniques require manual calibration [26–28].

For both linear and nonlinear regression models, the coupling of the regression coefficients is essential. Linear regression is used when a linear relationship exists between the input and the expected outcomes [29]. Compared to a nonlinear regression model, a linear model can more precisely illustrate the relationship between the required performance of the concrete and formulation components; however, it can be difficult to correlate data with complex relationships [30]. Regression models have been investigated as viable substitutes for repeated trials in a number of engineering disciplines during the last few decades. Using

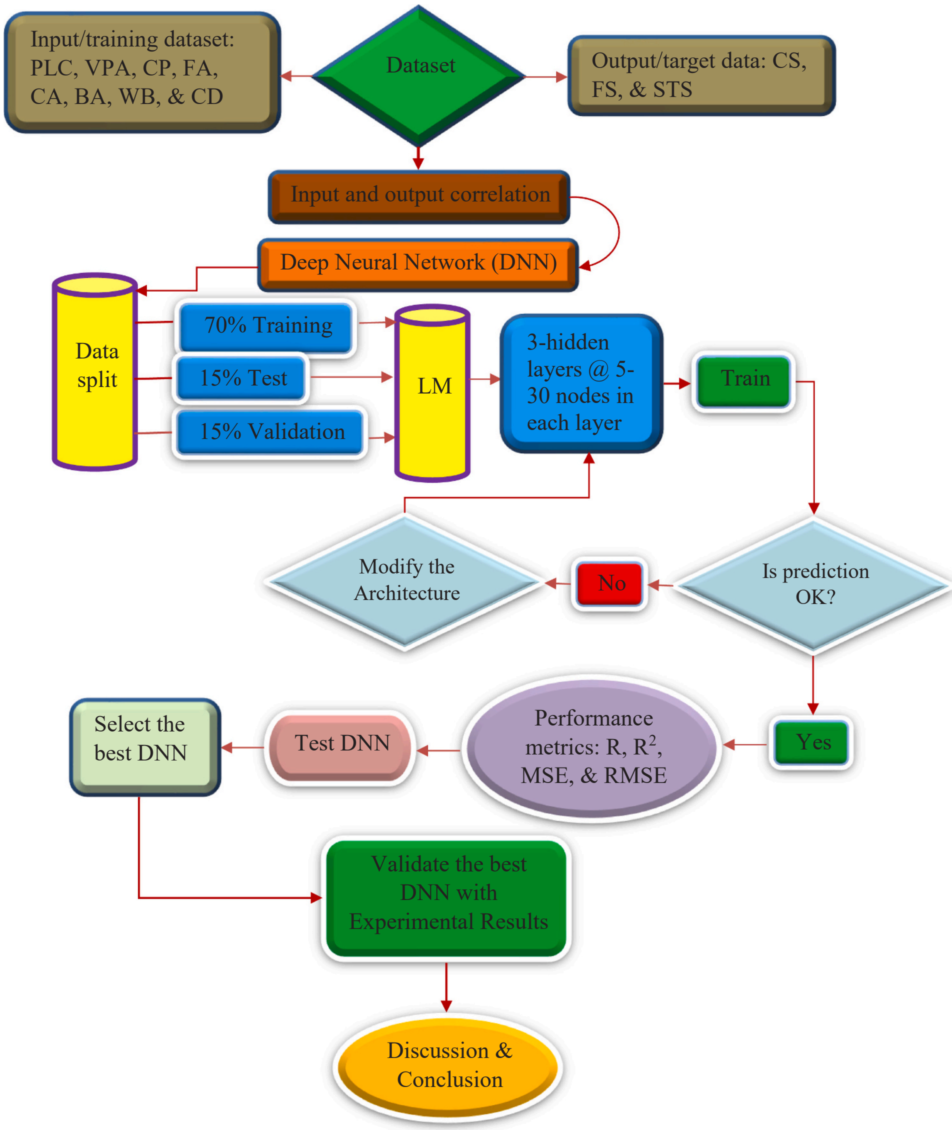

Fig. 6. DNN's flowchart.

machine learning (ML) approaches such as support vector machines (SVMs) and artificial neural networks (ANNs), nonlinear regression models have been built to estimate the concrete strength [31–34]. The relationship between the design mix proportions and the required concrete performance can be deciphered and examined through the application of nonlinear regression models in machine learning. However,

it requires a lot of time and effort to analyze large amounts of high-dimensional data, and the engineer (user) must specifically choose the analysis approach for pattern detection [35,36]. Moreover, high cost and time consumption restrict the suitability of statistical models for forecasting intricate systems [37].

Many attempts have been made to incorporate neural networks that correctly extract high-level features from complex data by using pre-existing ML models that account for associated factors like concrete mix design parameters [38,39]. ANN, decision trees (DT), ensemble of trees (ET), Gaussian process regression (GPR), gene expression programming (GEP), random trees (RT), SVM, and other ML techniques are the most widely used techniques for predicting concrete strength with promising results [40–43]. For example, SVM was used to forecast the compressive strength of high-performance concrete (HPC) with respect to the input variables (cement, fly ash, ground blast furnace slag (GBFS), aggregates, water, and superplasticizer) with total dataset of 1030 [30,44]. DT was engaged to predict the CS and ultrasonic pulse velocity of concrete in respect to the input variables (cement, GGBS, fly ash, silica fume (SF), water, aggregates, and curing day) with a dataset of 40 and 30-fold cross validation [45]. RF was employed to forecast the CS of HPC with respect to the input variables (water-binder ratio (WB), GBFS/W ratio, fly ash/W ratio, coarse aggregate (CA)/B ratio, and CA/fine aggregate (FA) ratio) [46]. Nevertheless, ML/DL models with improved updating capabilities and the capacity to evaluate big datasets outperform experimental models [37]. According to ML techniques, various factors should be considered while choosing the right model to forecast the target strength of concrete. The correlation between the mechanical strength of the concrete and its constituents influences the forecasting model selection [37]. Thus, in the event that the relationship is nonlinear, models with nonlinear space response capabilities ought to be employed. Thus, SVM and ANN models can be applied in these situations because of their appropriate performance and lower error rates in non-linear environments [37]. However, relatively little research has been done on the use of deep neural network to predict the mechanical characteristics of ternary blended concrete.

Deep neural network (DNN) techniques have gained popularity as efficient and cost-effective methods to predict how a material's property influences the quality, cost, and time of concrete mixes. Deep neural

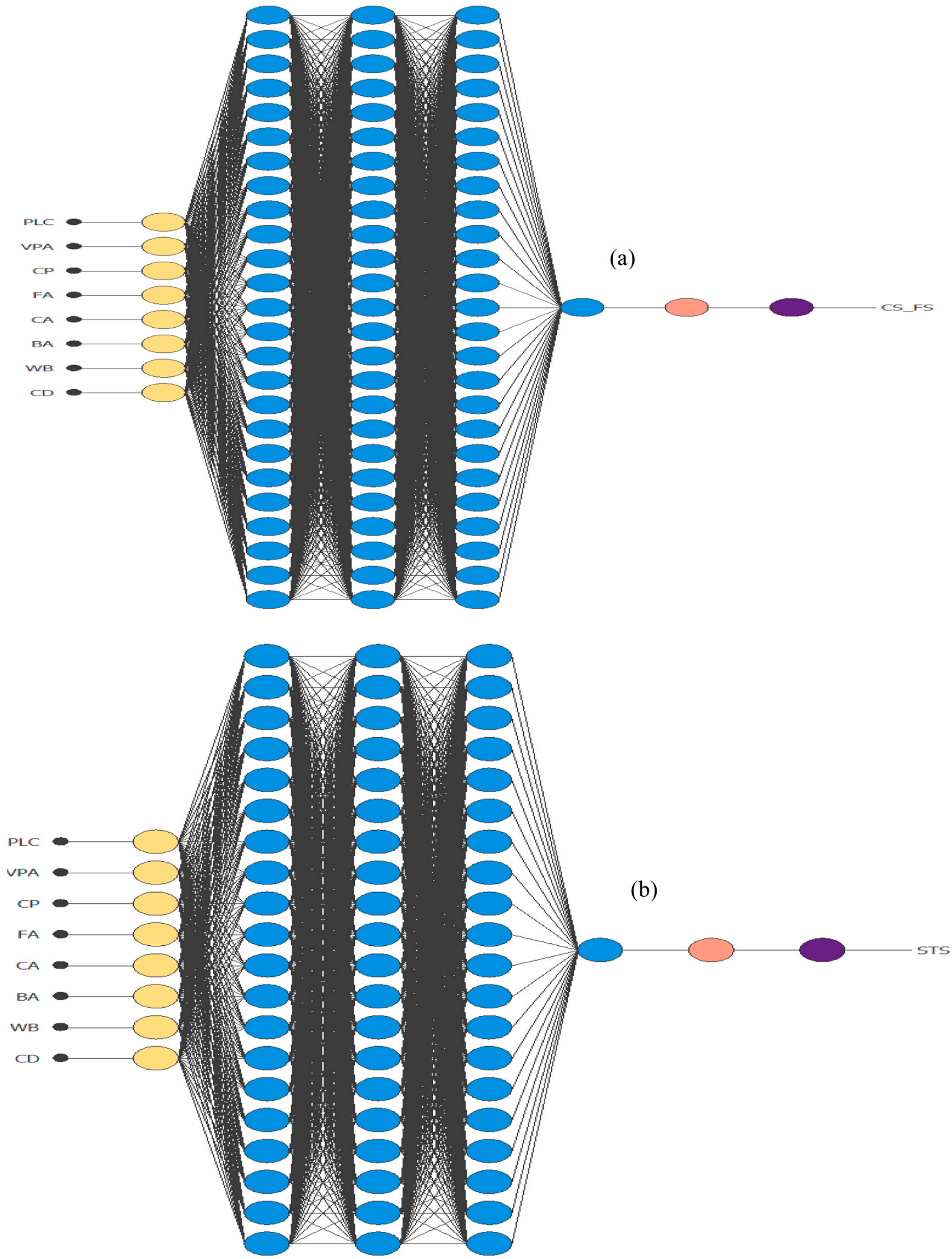

Fig. 7. Graphical representation of the best DNN architectures for (a) CS and FS (8–25–25–25-1) and (b) STS (8–20–20–20-1).

network methods are useful for large-scale, multidimensional data analysis [47]. Deep Learning (DL) is a special type of machine learning approach that can extract the optimum input directly from raw data without any human intervention [48,49]. Deep learning algorithms can thus help with the process of extracting features as well as the correlations between features and the desired output. In the end, without feature extraction, the DL approach can, with appropriate training, establish direct mapping from main or raw inputs to the desired outputs [49–51]. It can also locate the high-level attributes as a hierarchy that elucidates the low-level learned attributes. This characteristic allows DL algorithms to break down challenging jobs into easier ones and solve them [48,49,52]. A related work that demonstrated the efficacy of DNN

Table 4
Statistical analysis of mechanical datasets.

Factor	Unit	Minimum	Maximum	Mean	Median	SD	Variable
PLC	Kg/m^3	228	332	277.88	277	33.45	Input
VPA	Kg/m^3	16.5	55.5	34.81	34.75	14.26	Input
CP	Kg/m^3	16.5	55.5	34.81	34.75	14.26	Input
FA	Kg/m^3	802	857	829.24	830	20.34	Input
CA	Kg/m^3	919	919	919	919	0	Input
BA	Nil	0.18	0.22	0.20	0.20	0.016	Input
WB	Nil	0.54	0.61	0.58	0.58	0.035	Input
CD	Day	3	120	52.01	60	43.21	Input
CS	MPa	6.88	37.33	24.44	25.73	8.50	Output
FS	MPa	1.44	5.36	3.58	3.85	1.03	Output
STS	MPa	0.85	3.38	2.32	2.44	0.68	Output

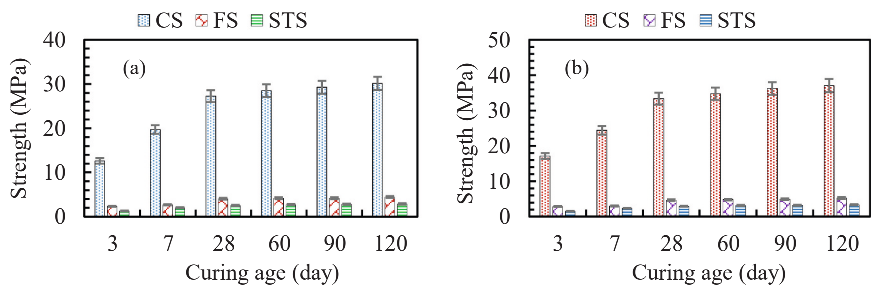

Fig. 8. CS, FS, and STS of control concrete for (a) C 25 MPa and (b) C 30 MPa.

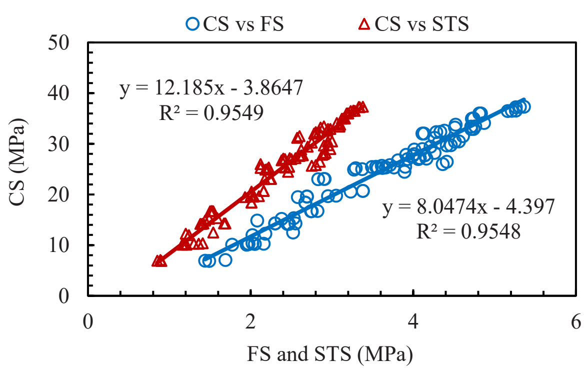

Fig. 9. Relationship between the CS and FS, and CS and STS.

techniques in predicting the mechanical strengths of geopolymer concrete based on mix proportions supports this [53]. However, existing DL approaches often use simple structures. Furthermore, some research exclusively employed values that have been hyper-tuned [47], and some studies examined the effects of hyper-parameter tuning [54–57]. Some research have made use of fixed datasets that have been referenced in literature [58,59]. The datasets utilized in related research, however, were from experimental works, and they are sizable and suitable for forecasting the mechanical characteristics of concrete [47]. Presently, to the best knowledge of authors, there is no research on the binary blend of VPA and CP in concrete production, despite the possibilities of using VPA and CP in concrete as cement alternatives for environmentally friendly concrete. This differentiates between the existing literature and the present study.

The study applies DNN techniques to develop nonlinear regression models that forecast the CS, FS, and STS of the on-site concrete in relation to input variables [cement content, VPA content, CP content, FA content, CA content, binder-aggregate ratio (BR), WB, and curing days (CD)]. By using a random stream function and an ideal network topology, the associated DNN models were optimized, improving performance. Experimental findings were used to obtain data for 108 ternary blended concrete (TBC) samples, with target CS values of 25–30 MPa. The DNN model structures with 3 hidden layers and 5–30 neurons in each layer were used to ascertain the best network architecture. The models were trained with 100 experimental datasets and evaluated using metric indicators. The model's accuracy was verified by testing the developed DNN model with 8 unobserved experimental values.

This study is original in that it blends two supplementary cementitious materials (SCMs), Vitellaria paradoxa ash and calcite powder, with PLC. This method would reduce these materials from landfills and leverage their pozzolanic and supplementary cementitious properties to significantly address resource and environmental problems and improve the mechanical strength of TBC. The significance of this research lies in its assurance of the application of the created DNN models in the building and construction industry for predicting the mechanical properties of concrete that incorporate SCMs without requiring any experiment, saving time and cost.

2. Materials and methods

2.1. Materials

Portland limestone cement (PLC, 42.5 R) that complies with BS 197–1 [60], as shown in Fig. 1, was used. Shea nutshells and CP were locally obtained from Agbonle and Lagos, Nigeria. The nutshells were sun-dried for 7 days to aid the valorization processes. After that, the nutshells were calcined at 700 °C for 3 h under a control condition, obtaining about 30 wt% VPA shown in Fig. 1. After that, a 45-μm BS sieve was used to filter the VPA. Granite, with a maximum particle size of 12.5 mm, was utilized as CA. River sand having a maximum particle size of 4.75 mm, was used as FA. All aggregates used satisfied the BS requirements [61]. Binding materials were evaluated for specific gravity (SG) and bulk density (BD) as per BS [62]. Table 1 shows the physical properties of materials used. Table 2 presents the chemical compositions of PLC, VPA, and CP as analyzed by an XRF analyzer (JOEL-JSM 7600 F).

Table 2 shows that CP and VPA satisfied ASTM pozzolanic standards [63], where the LOI was less than 6 %, and the combined amount of silica, alumina, and ferrite was more than 50 %. Since the CaO concentration of CP was more than 18 %, it is designated as Class C

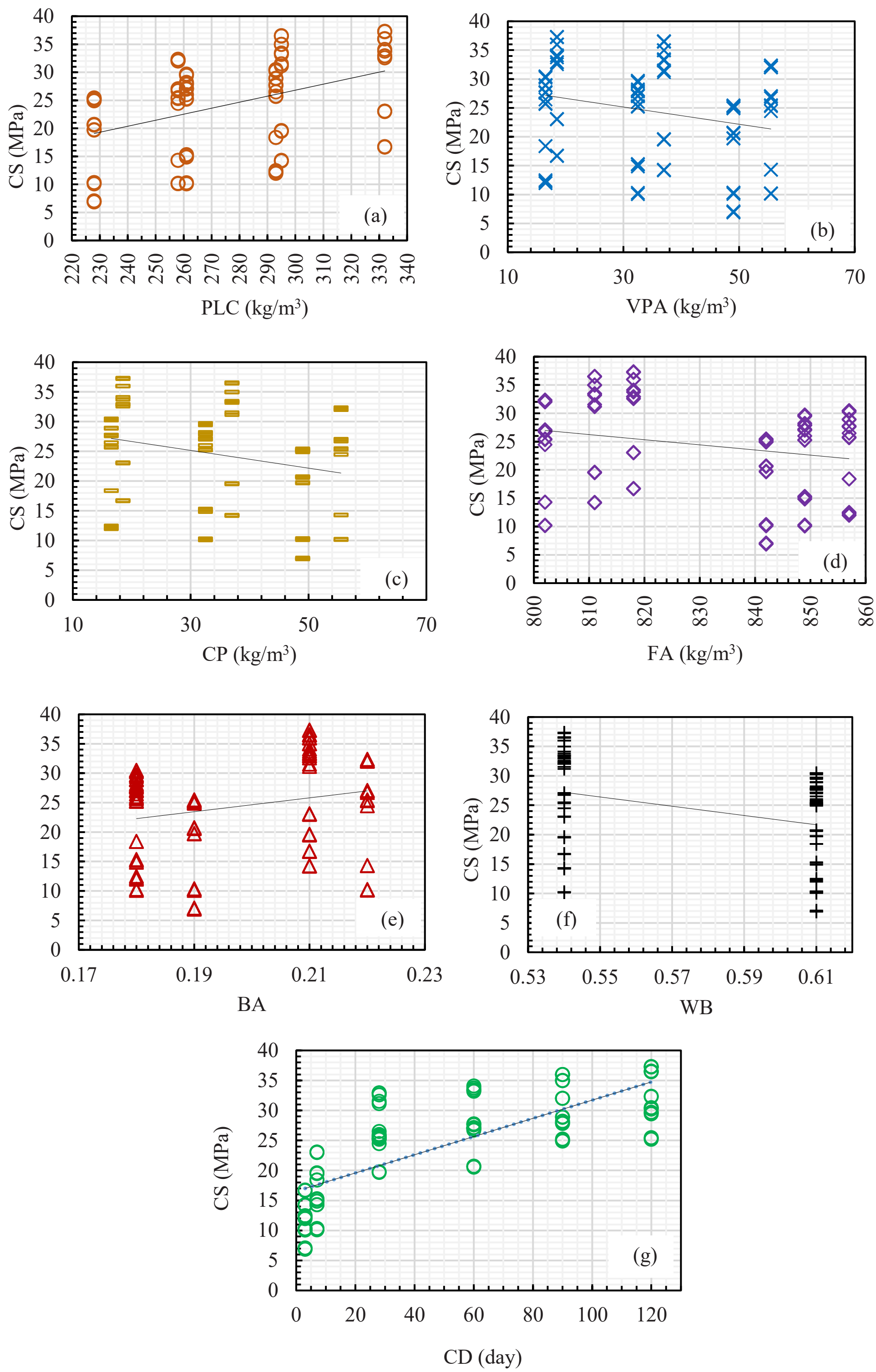

Fig. 10. Response between target (CS) and (a) PLC, (b) VPA, (c) CP, (d) FA, (e) BA, (f) WB, and (g) CD.

Pozzolan; in contrast, the CaO level of VPA is classified as Class F Pozzolan.

Fig. 2 shows the binding materials' particle size distribution (PSD) as determined by laser diffraction using a Beckman Coulter LS-100 model. The aggregate grades, as defined by the BS [61], is shown in Fig. 3 together with the lower limits (LL) and upper limits (UL).

2.2. Experimental methods

The ACI specification [64] is utilized in this research to design the proportions of the concrete samples with specified compressive strengths of 25 and 30 MPa. For all specimens in this study, the W/B ratios were set at 0.61 and 0.54 for 25 and 30 MPa to attain slump values between 25 and 50 mm [64]. Based on the unit weights, the control mix (VC0) consisting of 0 wt% VPA and CP was created for a volume of 1 m^3. Although a range of 5–10 wt% of VPA and CP have been recommended

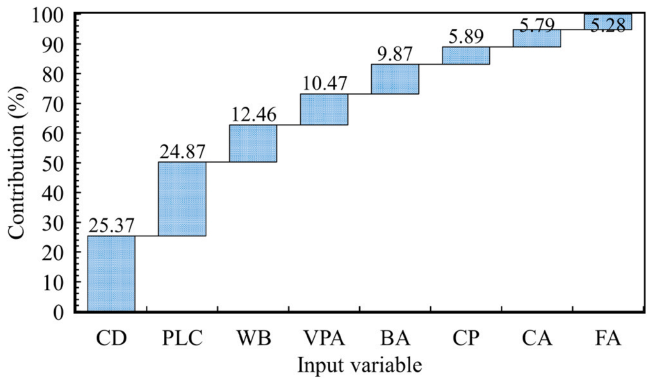

Fig. 11. Sensitivity analysis of each input variable on the output variable.

as cement replacements for concrete manufacturing to achieve better mechanical, durability, and sustainable properties [1,65]. Notwithstanding, this research extended the replacement by preparing three TBC samples (VC5, VC10, and VC15), substituting PLC with 5, 10, and 15 wt% VPA and CP. The quantity of mix design proportions is shown in Table 3.

Various combinations of specimens were made and examined in compliance with the procedure specified by the BS [66] to determine the CS of concrete samples. The different concrete mixtures are moulded using cubes measuring 100 mm × 100 mm × 100 mm [67]. A 500 mm × 100 mm × 100 mm prismatic beam was used to assess the concrete's FS as per BS's specification [68]. Concrete's STS was carried out in compliance with BS [69] using the 200 mm high with 100 mm diameter cylindrical moulds. All concrete samples were cured by immersion in water at 23 ± 5 °C and 65 ± 5 % relative humidity. Samples of cubes, cylinders, and beams for CS, STS, and FS tests are shown in Fig. 4. A trio of samples was used for each blended sample.

2.3. DNN

To investigate the mechanical properties of the concrete by experimental testing, time and resources are required. Because of the impact of multiple factors, such as geology, mineralogical compositions, and production techniques and procedures unique to each concrete constituent, it is difficult to precisely estimate the qualities of concrete. As a result, AI methods are needed to do this. A subset of AI called DNN has gained enormous traction in scientific and technical computing, where its techniques are used to solve challenging problems. Currently, the multilayer perceptron, the most common kind of neural network, is trained using the backpropagation technique [70]. One way to train a two-layer network to replicate most functions accurately is to utilize a two-layer sigmoid. Typically, two or three hidden layers are adequate in practical neural networks. The use of four or more layers is unusual [70–72]. Research on DNN's optimizers such as Levenberg Marquardt (LM), scale conjugate gradient (SCG), and Bayesian regularization (BR) [73] and 2–4 hidden layers [74–76] demonstrated the superior performance metrics for LM and the third hidden layer in comparison to other optimizers and hidden layers. Thus, this research engaged a 3-hidden layer network with 5–30 neurons per layer.

2.3.1. Model training and testing

The training and target datasets were loaded using a code created in MATLAB R2021a. While the training dataset had PLC, VPA, CP, FA, CA, BA, WB, and CD findings, the target dataset contained CS, FS, and STS values. The network was trained using training and target datasets using LM ('trainlm') as the learning algorithm. The network was designed with 3 hidden layers and 5–30 nodes per layer to determine how different neurons affect DNN topology and to choose the best DNN structure for predicting the CS, FS, and STS of concrete. In this configuration, the first network's output serves as the second network's input and the second network's output serves as the third network's input. This shows that in a multilayer network, the output of one layer becomes the input for the layer that follows it. Eq. (1) provides an illustration of this procedure [70]. There may be variations in the transfer function as well as the total number of neurons in each layer. Eq. (2) thus displays the third network's output [70].

$$a^{m+1} = f^{m+1}\left(W^{m+1}a^m + b^{m+1}\right) form = 0, 1, \ldots, M-1 \quad (1)$$

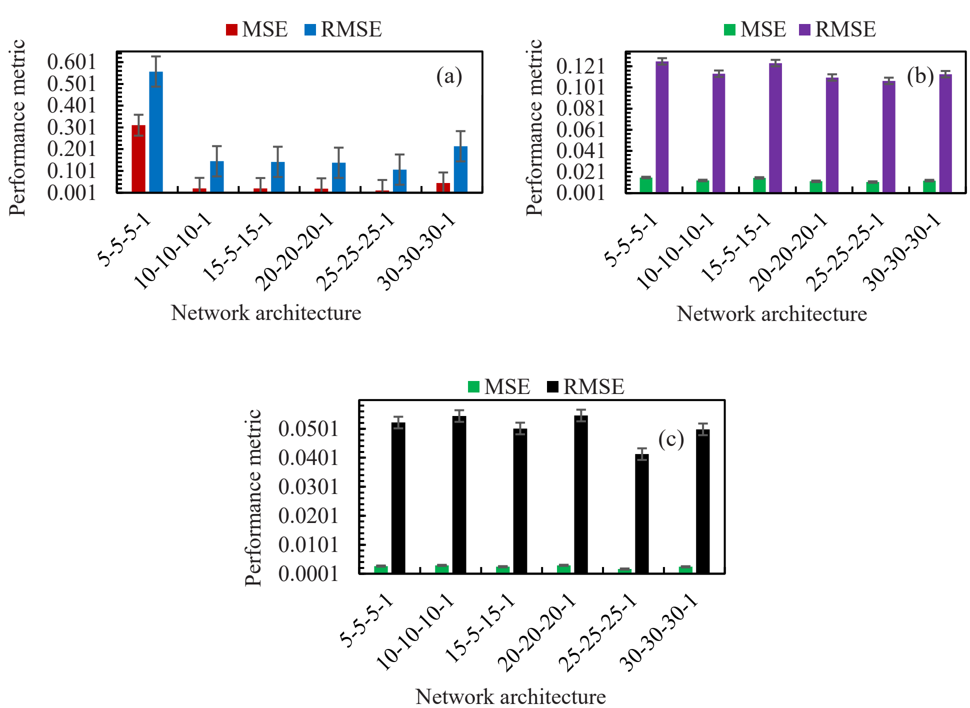

Fig. 12. MSE and RMSE for (a) CS, (b) FS, and (c) STS.

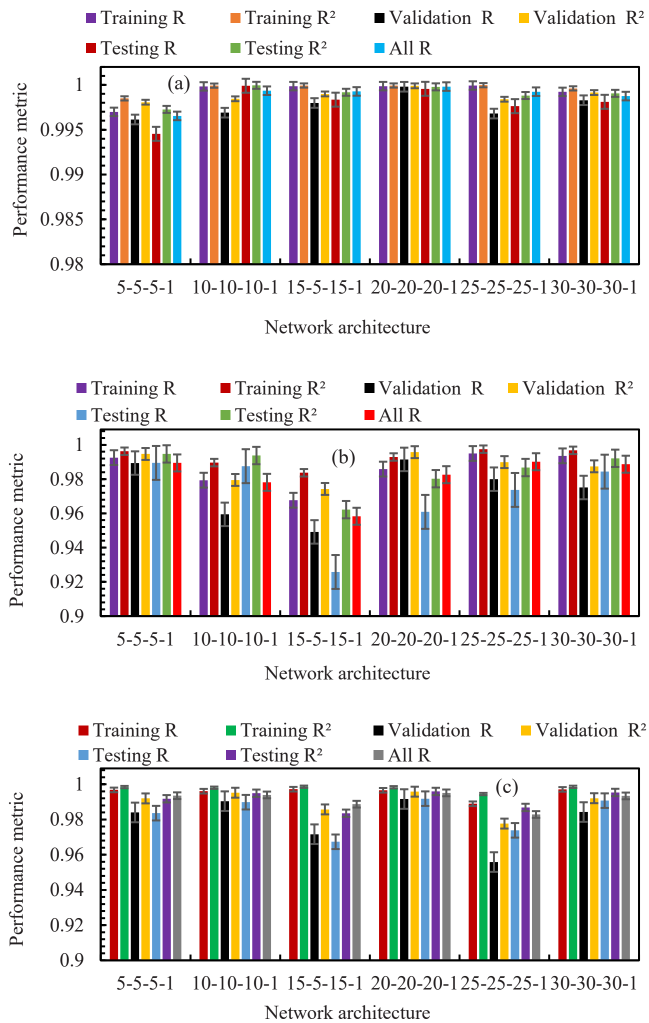

Fig. 13. R and R^2 values for (a) CS, (b) FS, and (C) STS.

$$a^3 = f^3\left(W^3 f^2\left(W^2 f^1\left(W^1 p + \quad b^1\right) + b^2 + b^3\right)\right) \tag{2}$$

The neurons in the first layer receive inputs from outside sources, as per Eq. (4). This provides the initial value for Eq. (3).

$$a^0 = p \tag{3}$$

The outputs of the neurons in the final layer, as indicated by Eq. (4), are known as the network outputs.

$$a = a^M \tag{4}$$

where *a, f, m, p, W, and b* represent output vector, transfer function, network layers, input vector, weight matrix, and bias vector.

The DNN model can be prone to overfitting due to the additional classes of abstraction that enable rare-dependent training of datasets [26]. For this reason, a random stream (fitted function) was applied to prevent overfitting [53,74,76]. Additionally, this stream guarantees that the network always produces the same output after training.

The fitness function was used to build the network structure and learning algorithm. For each strength, CS, FS, and STS, 108 datasets were produced from the experimental research. Of these datasets, 96.6 % (or 100 data) were used for learning, while the remaining 7.4 % (or 8 datasets) were used as untrained datasets to confirm the accuracy of the models that were constructed. For training, validation, and testing, 70, 15, and 15 % of the learning datasets were utilized, respectively. The data division matrix was displayed in Fig. 5. In the end, the network was trained using the relation displayed in Eq. 5:

$$[P, \quad R] = t[X, \quad Y', \quad Z'] \tag{5}$$

where *P, R, t, X, Y, and Z* connote predictor, record, train, network, training dataset, and target dataset.

2.3.2. Validation of developed models

To ascertain model uncertainty, the best approach is to validate model predictions against observations made under various conditions. Complete set design proportion validation has not been carried out very often, despite being a crucial component of concrete strength forecasting. Generally, validation research has been limited to evaluating the components of the binary blend assessment model over a brief period [45,77–79]. Over the complete range of conditions that call for model predictions, little to no validation has been done. Such extensive validation requires significant time and money. This is why model validation has not received much attention in research. Model validation can often be almost difficult because of either extremely low levels of the spectrum of conditions or excessively extensive periods that the model considers. Thus, 8 datasets from the experimental results covering the full range conditions were used as untrained datasets to verify the accuracy of the developed models.

2.3.3. Evaluation of performance indicator

The precision of models was verified using R (correlation coefficient), R^2 (coefficient of determination), MSE (mean square error), and RMSE (root mean square error). These are illustrated in Eqs. (6)-(9). Mathematically, DNN models are more accurate when R and R^2 values are around 1, and MSE and RMSE values are around 0. The models were verified by performance plot, training state, histogram, and regression outputs. Eqs. 10 and 11 were used to validate the developed DNN. Fig. 6 displays the DNN flowchart procedure. The best DNN models are represented graphically in Fig. 7(a) and (b). They depict the best DNN structures for CS and FS, and STS. Fig. 7(a) consists of input layers having 8 input variables (PLC, VPA, CP, FA, CA, BA, WB, and CD), 3 hidden layers with 25 neurons in each layer, and an output or target variable (compressive strength). This architecture also yielded the best performance metrics for FS. However, Fig. 7(b) consists of input layers having 8 input variables (PLC, VPA, CP, FA, CA, BA, WB, and CD), 3 hidden layers with 20 neurons in each layer, and an output or target variable (split tensile strength).

$$R = 1 - \frac{\sum_{i=1}^{n}\left(y_i^{pred} - \quad y_i^{true}\right)}{\sum_{i=1}^{n}\left(y_i^{pred} - \quad \overline{y_i^{true}}\right)} \tag{6}$$

$$R^2 = 1 - \frac{\sum_{i=1}^{n}\left(y_i^{pred} - y_i^{true}\right)^2}{\sum_{i=1}^{n}\left(y_i^{pred} - \overline{y_i^{true}}\right)^2} \tag{7}$$

$$MSE = \frac{1}{n}\sum\nolimits_{i=1}^{n}\left(y_i^{pred} - \quad y_i^{true}\right)^2 \tag{8}$$

$$RMSE = \quad \sqrt{\frac{1}{n}\sum\nolimits_{i=1}^{n}\left(y_i^{pred} - \quad y_i^{true}\right)^2} \tag{9}$$

$$function[CS, FS, or\ STS] = n[P, \quad D] \tag{10}$$

$$CS, FS, or\ STS = P(D') \tag{11}$$

where n and D represent test network and data.

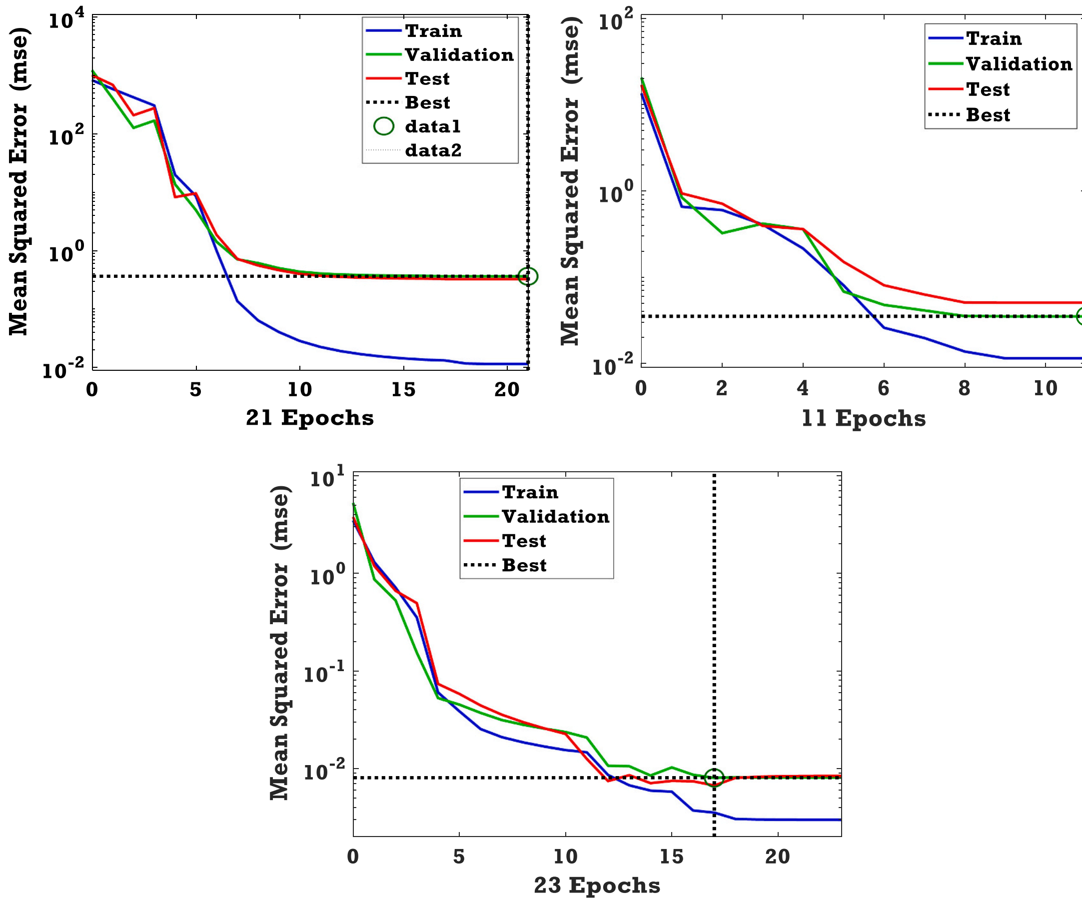

Fig. 14. Best validation performances for (a) CS, (b) FS, and (c) STS.

2.4. Sensitivity analysis

It is imperative to comprehend which variables have the greatest influence on model predictions. The derivatives of a model's outputs with respect to its inputs were computed to achieve this. Greater significance is indicated by high derivative values, and smaller significance is indicated by values near zero [80,81]. Sensitivity analyses are a useful tool for gauging the possible significance of model parameters as sources of uncertainty in model predictions when faulty model formulation is not anticipated to be a significant issue [80]. Machine learning requires numerous tests to evaluate and confirm the quality and dependability of the created model on a range of data sets. Improvements in the prediction model's accuracy and efficacy throughout training, testing, and validation of available data sets may not imply or promise improved performance in the end [77]. Consequently, Eqs. (12) and (13) are engaged to evaluate the relative importance of the variables that explained the outcome (CS):

$$Range_{output} = Max(\overline{x}_{output}) - Min(\overline{x}_{output}) \tag{12}$$

$$SA = \frac{Range_{output}}{\sum_{i=1}^{p} Range_{output}} \tag{13}$$

where $Range_{output}$ defines the output range as the difference between the maximum and minimum CS output values observed when a parameter is changed while maintaining constant, the mean values of the other inputs; SA is sensitivity analysis.

3. Results and discussion

3.1. Statistical datasets

Table 4 displays the summary of statistical analysis and outcomes of the mix design proportions and strength values. Detailed raw datasets for CS, FS, and STS as well as code generation are freely available in Zenodo Repository at https://zenodo.org/doi/10.5281/zenodo.10998160.

Fig. 8 shows the mean CS, FS, and STS of the control concrete (VC0) using the identical mix design proportions. The results revealed that CS, FS, and STS of both concrete grades (C 25 and 30 MPa) increased with increasing curing ages. After 28 days curing, the CS, FS, and STS for C 25 MPa in Fig. 8(a) exhibited 27.25, 4.04, and 2.53 MPa, while that of C 30 MPa in Fig. 8(b) yielded 33.38, 4.66, and 2.88 MPa.

3.2. Relationship between the mechanical properties

There are similar patterns in the TBC's split tensile strength, compressive strength, and flexural strength. Fig. 9 indicates an increase in flexural and split tensile strengths with increasing compressive strength. A strong correlation exists between compressive strength and flexural strength with 95.48 % R^2. In the same vein, the relationship between the compressive strength and split tensile strength of ternary blended concrete yielded a robust correlation with 95.46 % R^2. These results corroborate a relevant study, which reported a strong correlation ($R^2 > 90$ %) between the CS and STS and CS and FS of blended concrete [1]. Ultimately, it can be inferred that the effects of input variables (PLC, VPA, CP, FA, CA, BA, WB, and CD) on compressive strength could also influence the flexural and split tensile strengths at 96 % confidence bound.

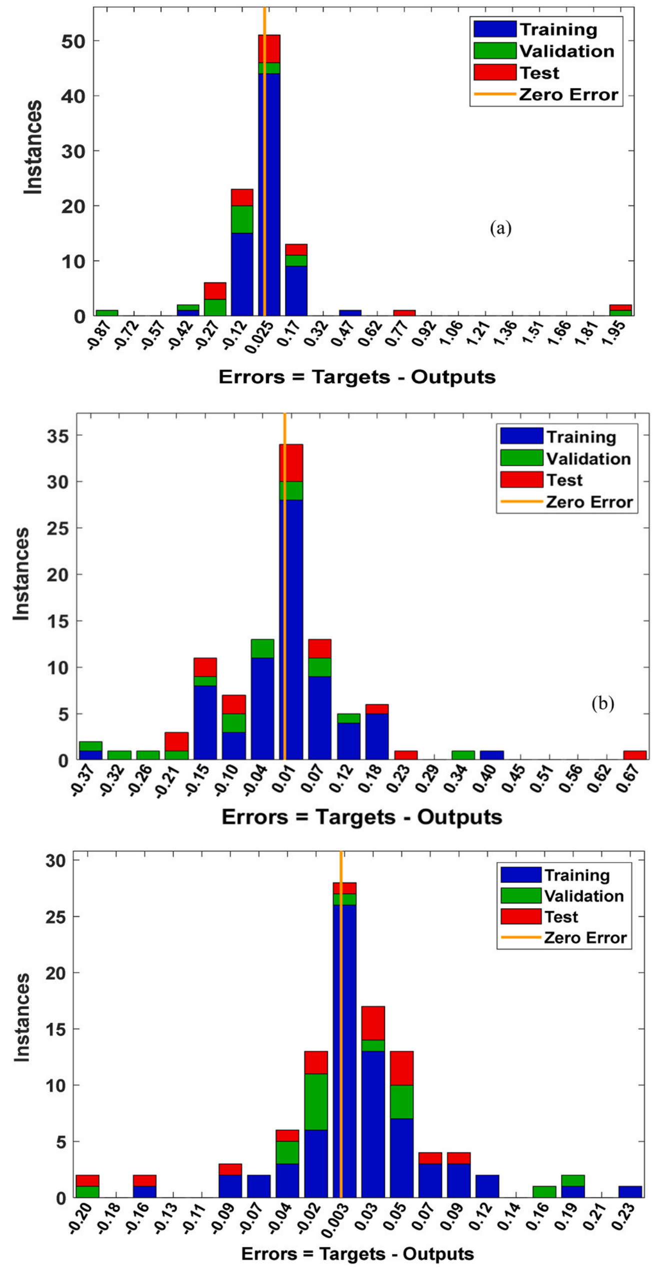

Fig. 15. Histogram errors for (a) CS, (b) FS, and (c) STS.

3.3. *Effects of input variables on compressive strength*

Fig. 10 (a)-(g) illustrate the contributions of each training (input) variable in the ternary blend to the target (output) variable, CS. As seen in Fig. 10 (a), an increase in PLC content causes an increase in CS. During the hydration phase, PLC particles react with water to generate the strength matrix and bind the aggregates. Cement hydrates to create phases of calcium hydroxide (CH) and alumina (C_3A). Alite (C_3S) and belite (C_2S) from cement pastes react with water to generate CH. CH is responsible for strength development [82,83]. As shown in Fig. 10 (b) and (c), the addition of VPA and CP at 5–10 % of PLC replacement (16.50–37 kg/m^3) enhanced TBC's CS and allowed it to meet the 25 and 30 MPa target strengths. A possible explanation for the increase in CS is the interplay between VPA/CP and the distributed CH during PLC hydration [1]. The strength improvement might also be a result of the cementitious chemicals that are produced when the added pozzolana (VPA) and PLC hydrate [1]. Furthermore, the addition of VPA allows silica (SiO_2) to react with the lime produced during cement hydration, producing additional cementitious chemicals that contribute to strength improvement. On the other hand, CP is a calcium carbonate crystal that is meta-stable and aragonite. It takes part in the hydration processes of blended cement. For instance, during cement hydration, it partially dissolves and precipitates, which appears to stabilize the production of ettringite, encourage the growth of calcium carboaluminate, and aid in the formation of Portlandite and other C-S-H matrix phases [84]. This has favorable effects on the hydration process, hydration products, and microstructure development in the blended cement system, which improve strength development. However, after a 10 % replacement, the strength started to decrease. High VPA and CP replacement levels reduce the PLC content. This decreases the amount of C-S-H gels from the hydration of PC at early ages and retards the strength development. This is in line with pertinent research, which found that the CS typically decreases as seashell powder content increases in blended cement mixes [84]. It also shows a strong correlation with the rise in the effective w/c ratio due to the substitution of seashell powder for cement. In blended cement mixtures, the modulus of C-S-H matrix phases typically decreases as seashell powder content rises [84]. Studies have shown that CS frequently decreases with increasing VPA content [1,85,86]. This is because the VPA's ability to delay PLC's early hydration slows down the potential for concrete to develop strength.

A drop in CS is seen in Fig. 10 (d) as the blended concrete's FA content rises. FA contributes very little to the prediction of CS because of its filling role [87]. Generally, concrete strength increases with decreasing aggregates in the mix due to the packing capability between the constituents. This supports the results depicted in Fig. 10 (d). Fig. 10 (e) indicates a rise in CS with decreasing BA content, strengthening the binding matrix (FA and CA) and causing early and later strength growth. The components of FA and CA did not appear to have a substantial impact on strength because pertinent research showed that aggregates' form, PSD, and ITZ had a greater effect on strength growth than their contents [88–90]. To enhance strength development, lower FA and CA levels, as well as higher paste volume, are also required [91].

Fig. 10 (f) demonstrates a decrease in CS with increasing WB. The reason for this is that as WB increases, capillary pores increase [92]. As a result, too much water will result in unwanted capillary pores in the concrete's mass. The porosity of concrete decreases with increasing porosity as the number of pores rises. The mass of the anhydrous cement increased as the hydration process went on, which caused the hydration product to increase. The hydrated product's incapacity to fully fill the capillary holes because of the increase in water-generated gel mass during the hydration process results in porous concrete. Fig. 10 (g) shows an increase in CS with increasing CD. This corroborates a study that reported an increase in the CS of blended concrete with increasing CD due to cement hydration [92]. Tricalcium silicate (C_3S) is the reason for the short time strength of 3 and 7 days because it combines with water easily to produce heat of hydration. CH is produced in greater amounts by C_3S and C-S-H in relatively lower amounts. Dicalcium silicate (C_2S), which hydrates considerably more slowly and generates less heat during hydration, is the cause of the cement's long-term strength enhancement, which lasts 28 days or more as it hydrates endlessly. There is less CH produced and the C-S-H created is denser [83,93,94].

3.4. *Sensitivity analysis*

Each input variable's effect on the strength of concrete prediction is displayed in Fig. 11. The input factors play a major role in the outcome projection. All of the input variables (CS) affected the target variable. With a contribution to the model's development of 25.37 %, the sensitivity analysis showed that CD is highly crucial in relation to the key variable's degree of significance. PLC, WB, and VPA came second, third, and fourth with percentage contributions of 24.87, 12.46, and 10.47 %, respectively. This is in line with the response results between the input and target variables in Fig. 8, which show that when WB and VPA

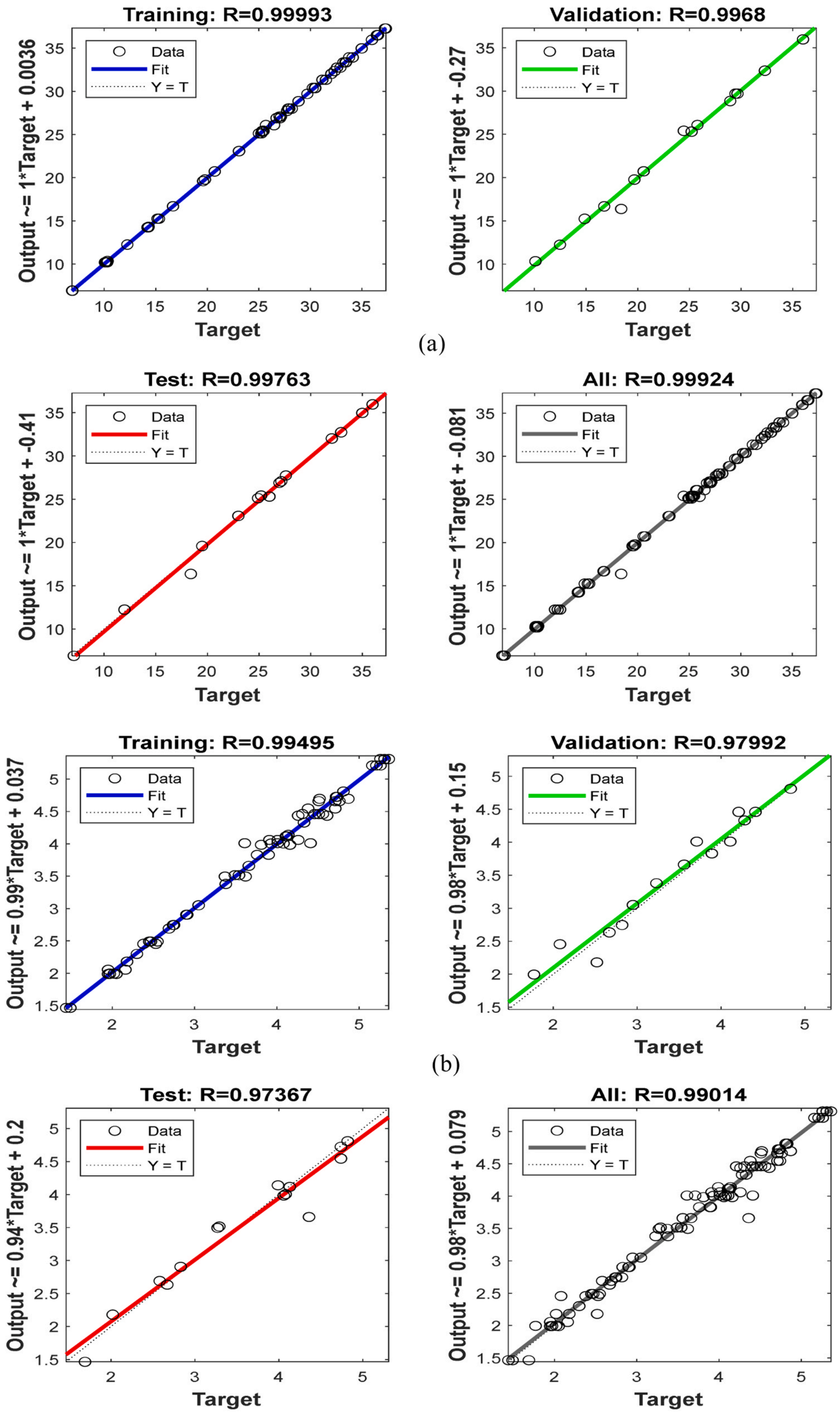

Fig. 16. Correlation between experimental and DNN approaches for (a) CS, (b) FS, and (c) STS.

decreased, and PLC and CD increased, the blended concrete's CS increased. Nevertheless, the remaining parameters had a smaller impact; specifically, the contributions from BA, CP, CA, and FA were 9.87, 5.89, 5.79, and 5.28 % to the TBC output variable. These outcomes are consistent with a prior study that found that the following factors affected the prediction of concrete's CS modified with SCMs: CD, PLC,

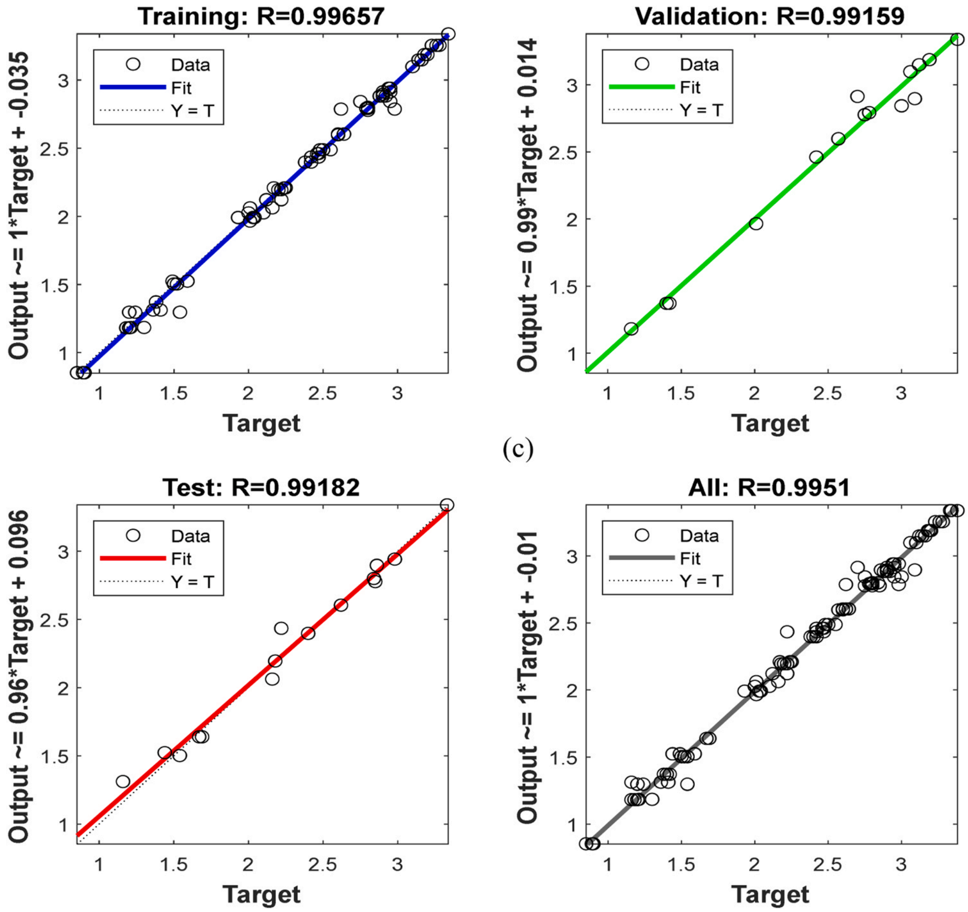

Fig. 16. (*continued*).

Table 5
Untrained experimental datasets and predicted values.

PLC CCA GOS FA CA (kg/m^3)					BA	WB	CD (days)	Experimental (MPa) CS FS STS			Predicted (MPa) CS FS STS		
261	32.5	32.5	849	919	0.18	0.61	3	9.96	2	1.20	10.19	2.06	1.19
293	16.5	16.5	857	919	0.18	0.61	7	18.10	2.37	2	17.96	2.29	1.97
228	49	49	842	919	0.19	0.61	28	20.47	3.75	2.20	19.77	3.65	2.13
293	16.5	16.5	857	919	0.18	0.61	90	29.20	4.36	2.97	28.85	4.18	2.85
258	55.5	55.5	802	919	0.22	0.54	7	14.15	2.16	1.70	14.3	2.30	1.64
295	37	37	811	919	0.21	0.54	28	31.41	4.51	2.65	31.34	4.44	2.60
332	18.5	18.5	818	919	0.21	0.54	60	34	4.77	3.13	33.93	4.70	3.10
258	55.5	55.5	802	919	0.22	0.54	120	32.4	4.38	2.86	32.35	4.33	2.80

Table 6
AB and RE between experimental and predicted variables.

Absolute error			Relative error (%)		
CS	FS	STS	CS	FS	STS
-0.23	-0.06	0.01	-2.31	-3.00	0.83
0.14	0.08	0.03	0.77	3.38	1.50
0.70	0.10	0.07	3.42	2.67	3.18
0.35	0.18	0.12	1.20	4.13	4.04
-0.15	-0.14	0.06	-1.06	-6.48	3.53
0.07	0.07	0.05	0.22	1.55	1.89
0.07	0.07	0.03	0.21	1.47	0.96
0.05	0.05	0.06	0.15	1.14	2.10

water, CA, blast furnace slag, fly ash, and FA contributed 27.8, 21.7, 11.5, 7.6, 6.1, 5.8, and 2.1 % to the strength development [95]. Another research found that water-total material ratio, recycled CA, FA, natural CA, and water-cement ratio are the most important parameters that influence the CS of concrete with 20, 17, 16, 14, and 13 % contributions [96]. Nonetheless, the evaluation of sensitivity depends on the number of input variables and data points utilized to train the model. Additionally, ML approaches have an impact on every variable; hence, different results are produced when additional input variables are introduced, and the proportions of the concrete mix are changed [95].

3.5. Performance metrics of DNN structures

The performance metrics used in the training, validation, and testing sets of the DNN are displayed in Figs. 12 and 13. The MSE, RMSE, R, and R^2 results demonstrated and supported the model's flexibility and validity for all network architectures. The results from Figs. 12 and 13 showed an improvement in performance as the number of neurons in the hidden layers increased, which is consistent with earlier studies [53,97]. The 8–25–25-25-1 network structure, as indicated in Fig. 12 (a) and (b),

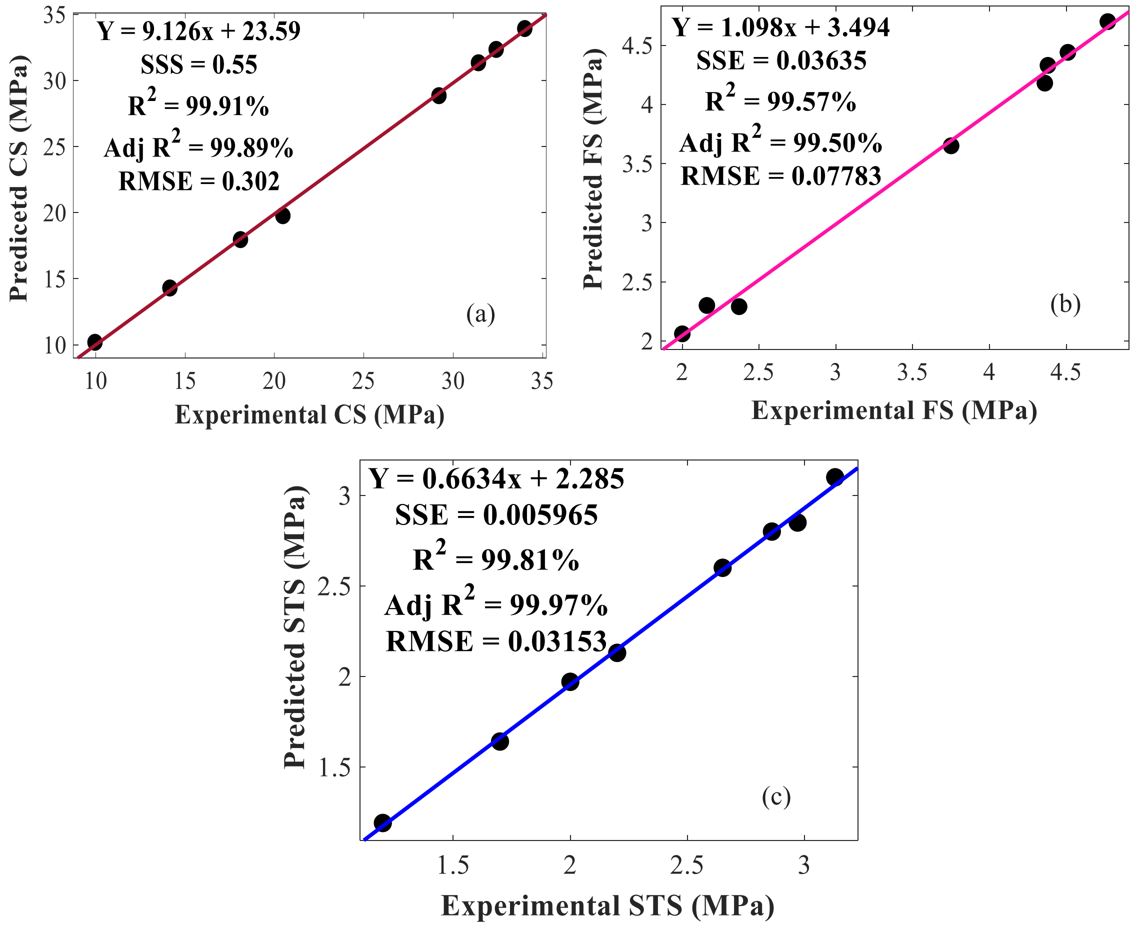

Fig. 17. Relationship between the predicted and experimental variables for (a) CS, (b) FS, and (c) STS.

outperformed other structures for training, validating, and testing with lesser MSE and RMSE values of 0.0115 and 0.107 for both CS and FS models. The MSE performance indicator of 8-25–25-25–1 network structure was about 40–96 % lower than other network architectures. However, the 8-20–20-20-1 network topology, as shown in Fig. 12 (c), produced the best metrics for predicting the STS of TBC. Higher R and R^2 values of 0.99993 and 0.99997 for training, 0.99680 and 0.99840 for validation, and 0.99783 and 0.99924 for testing in Fig. 13 (a) corroborate the CS' MSE and RMSE results. In the same vein, FS prediction, as indicated in Fig. 13 (b), exhibited the best R and R^2 of 0.99495 and 0.99747 for training, 0.97995 and 0.98992 for validation, and 0.97367 and 0.98675 for testing. Higher R and R^2 values with 0.99657 and 0.99828 for training, 0.99159 and 0.99579 for validation, and 0.99182 and 0.99590 for testing compared to other structures, as displayed in Fig. 13 (c), support the error performance metrics (MSE and RMSE). Strong correlation and accuracy of the model are indicated by lower values of the errors (MSE and RMSE) and higher values of the coefficients (R and R^2) [98]. Thus, it is clear from Figs. 12 and 1 that training, validating, and testing TBC datasets using a 3 hidden layers of 25 nodes for CS and FS, and 20 nodes for STS allowed the datasets to reach their optimal learning structures and produce optimal performance metrics. These findings can be associated with the generalization abilities of several layers, enabling them to learn all features between the input and target variables and perform advanced categorization.

The best DNN validation performance is displayed in Fig. 14 using the LM backpropagation training technique. The best validation results were 0.36418 for CS at epoch 21, 0.035188 for FS at epoch 11, and 0.0080441 for STS at epoch 17 in Fig. 14 (a)-(c).

In a similar vein, Fig. 15 shows the error difference between the expected and actual results, with the overall error range split into 20 smaller bins. Fig. 15 (a)-(c) demonstrate bins corresponding to the errors of 0.02471, 0.0125, and 0.002881 for CS, FS, and STS. At zero error in Fig. 15 (a) for CS, the highest bin height was about 50, with 88 % for training datasets, 2 % for validating datasets, and 10 % for testing datasets. The maximum bin height at zero error in Fig. 15 (b) for FS was around 34, with 82 % for training datasets, 7 % for validating datasets, and 11 % for testing datasets. At zero error in Fig. 15 (c) for STS, the highest bin height was about 28, with 88 % for training datasets, 6 % for validating datasets, and 6 % for testing datasets. Fig. 16 displays the evaluation of the direction and intensity of the linear correlations between the target and expected parameters. With strong correlation coefficients of 99.924, 97.992, and 99.510 % at 95 % confidence level and prediction intervals shown in Fig. 16 (a)-(c), the developed DNN structures are able to predict the CS, FS, and STS, and are judged to be dependable, accurate, and outstandingly performed.

3.6. Validation of developed DNN architectures

The validation process employed raw datasets from the experimental works to further demonstrate the capabilities of the 8–25–25–25-1 structure for CS and FS and 8-20–20–20-1 topology. Table 5 presents the correlation between the actual and anticipated strengths along with the corresponding absolute errors (AB) and relative errors (RE) in Table 6. Experimental values were normalized by mean and standard deviation of 23.71 and 9.206 for CS, 3.537 and 1.166 for FS, and 2.339 and 0.6795 for STS, with 95 % confidence bound. Fig. 17 presents the verification of predicted results against experimental data. It is evident, therefore, that the created DNN models learned and accurately predicted the experimental data with 99.91, 99.57, and 99.81 R^2 for CS, FS, and STS in Fig. 17 (a)-(c). This also implies that the newly created DNN models are robust and capable of accurately reproducing the experimentally observed results with remarkably high accuracy, given the explanatory model parameters. Additionally, the developed models are able to understand the relationship between various design parameters and the responses to the outcomes. Moreover, the performance indicators, 0.3021, 0.07783, and 0.03153 RMSE pertaining to CS, FS, and STS in Fig. 17 (a)-(c), exhibit a high degree of comparability, with minimal differences that show the model's overall efficacy. The validation of developed GEP model with the datasets from previous studies reported the RMSE above 1, demonstrating wavering forecast accuracy [77]. However, in the model validation of green concrete incorporating GGBFS and CCA, the R^2 and RMSE values for the projected response using raw experimental datasets were 0.9861 and 1.4180 for CS, 0.9811 and 0.1342 for FS, and 0.9694 and 0.1160 for STS [53]. Therefore, it is evident from Fig. 17 (a)-(c) that the created models are able to forecast the concrete's CS, FS, and STS.

The predicted CS and FS with 8-25–25-25-1 network architecture, and STS of TBS with 8-20–20-20–1 topology, as shown in Table 6, exhibited error lines within −2.31 and +3.42 % for CS, −6.48 and +3.38 % for FS, and +0.83 and +4.04 % for STS for validating the developed DNN structures. The reliability of the proposed models was clearly shown by very little difference between experimental and projected values. Thus, the created models are suitable and passably accurate.

4. Conclusions

This research investigates the development of DNN-based AI technique to evaluate and forecast the mechanical strengths of TBC. TBC strengths were predicted using DNN models in the range of 6.88–37.33 MPa for CS, 1.44–5.36 MPa for FS, and 0.85–3.38 MPa for STS. The developed models were predicated on extensive and dependable datasets on TBC's CS, FS, and STS that were acquired via a number of experimental works involving important mix design variables. The investigation yielded the following conclusions:

The addition of VPA and CP enhanced TBC's CS, FS, and STS. However, 28-day curing strength targets were met at 10 % VPA and 10 % CP replacements. All input variables significantly influence the CS, FS, and STS of TBC with CD, PLC, WB, and VPA contributing about 26, 25, 13, and 11 %. The relationship between the CS and FS, and CS and STS yielded strong correlation with 95.45 % R^2. Furthermore, the 8–25-25-25-1 network topology demonstrated the best prediction accuracy in forecasting the TBC with R and MSE of 99.92 % and 0.012 for CS and 99.01 % and 0.012 for FS. Thus, there was about 40–96 % and 6–27 % reduction in MSE when 8–25–25-25-1 network architecture is engaged in predicting the CS and FS of TBC compared to other network structures. The 8–20-20-20-1 outperformed other network architectures in properly predicting the STS of TBC, generating R and MSE of 99.51 % and 0.0030. With the developed DNN structures, the predicted CS, FS, and STS were found to be accurate with the experimental values, yielding 99.91, 99.57, and 99.81 % R^2. Ultimately, validating the developed models with untrained datasets highlights the remarkable performance of the 8-25–25-25-1 and 8–20–20–20-1 network architectures with RMSE values of 0.30 for CS, 0.078 for FS, and 0.032 for STS.

This study provides theoretical and practical recommendations for optimization of concrete mix proportion that maximizes efficiency and saves time. More industrial and agricultural waste materials might be used for TBC rather than being irresponsibly dumped in landfills and dumps since the built and verified models can recreate accurate and realistic outcomes. It is advantageous to make TBC with RWMs because it addresses environmental and resource challenges. These encourage sustainable and ecologically friendly building practices.

5. Future recommendations

Metaheuristic algorithms, such as nuclear reaction optimization and lightning search algorithm are recommended to predict the strength of concrete, as these techniques can produce also accurate results. Further input parameters can be included, such as the concrete's slump, density, and chemical and physical characteristics of the ingredients. One way to improve the accuracy and responsiveness of the models is to add more variables. Additional strength and durability characteristics of TBC, including resistance to carbonation, sulfate, acid, and chloride, can be predicted using machine learning techniques. Furthermore, sensitivity analysis (SA) was used in this study to determine the impact of each variable on the TBC strengths. However, the SHAP methodology can be applied and contrasted with the SA results.

CRediT authorship contribution statement

Solomon Oyebisi: Writing – review & editing, Visualization, Software, Resources, Methodology, Investigation, Funding acquisition, Formal analysis, Data curation, Conceptualization. **Thamer Alomayri:** Writing – original draft, Visualization, Resources, Funding acquisition.

Declaration of Competing Interest

The authors show a credit to the sources in the manuscript. The authors declare that they have no known competing for financial interests or personal relationships that could have appeared to influence the work reported in this paper. The raw/processed data required to reproduce these findings cannot be shared at this time as the Data also forms part of an ongoing study. The authors declare that the manuscript is the authors' original work and has not been published before. The authors also declare that the article contains no libelous or unlawful statements and does not infringe on the rights of others.

Data Availability

All data used are included in the manuscript. Open access repository is made for raw datasets and code generation.

References

[1] J. Ahmad, M.M. Arbili, H. Alabduljabbar, A.F. Deifalla, Concrete made with partially substitution corn cob ash: a review, Case Stud. Constr. Mater. 18 (2023) e02100, https://doi.org/10.1016/j.cscm.2023.e02100.

[2] International Atomic Energy Agency, Radiation Protection and Safety of Radiation Sources: International Basic Safety Standards, Vienna, 2014. ⟨https://www-pub.iaea.org/MTCD/publications/PDF/Pub1578_web-57265295.pdf⟩ (accessed 20 October 2022).

[3] F. Farooq, X. Jin, M. Faisal Javed, A. Akbar, M. Izhar Shah, F. Aslam, R. Alyousef, Geopolymer concrete as sustainable material: a state of the art review, Constr. Build. Mater. 306 (2021) 124762, https://doi.org/10.1016/j.conbuildmat.2021.124762.

[4] I.Y. Hakeem, M. Amin, I.S. Agwa, M.H. Abd-Elrahman, O.M.O. Ibrahim, M. Samy, Ultra-high-performance concrete properties containing rice straw ash and nano eggshell powder, Case Stud. Constr. Mater. 19 (2023) e02291, https://doi.org/10.1016/j.cscm.2023.e02291.

[5] A.A.J. Ghanim, M. Amin, A.M. Zeyad, B.A. Tayeh, I.S. Agwa, Effect of modified nano-titanium and fly ash on ultra-high-performance concrete properties, Struct. Concr. 24 (2023) 6815–6832, https://doi.org/10.1002/suco.202300053.

[6] S. Oyebisi, T. Alomayri, Cement-based concrete modified with Vitellaria paradoxa ash: A lifecycle assessment, Constr. Build. Mater. 342 (2022), https://doi.org/10.1016/j.conbuildmat.2022.127906.

[7] Mbakbaye, et al., Potential use of shea nutshell ash as partial replacement of Portland cement in interlocking earth blocks, Int. J. Adv. Technol. Eng. Explor. 9 (2022), https://doi.org/10.19101/IJATEE.2021.875482.

[8] P. Zievie, P.P.K. Yalley, H. Danso, K. Antwi, Assessing the strength and durability behaviour of concrete enhanced with kaolin clay and Shea nut shell particles, Cogent Eng. 11 (2024), https://doi.org/10.1080/23311916.2024.2321384.

[9] A.N. Adazabra, G. Viruthagiri, R. Ravisankar, Cleaner production in the Shea industry via the recovery of Spent Shea Waste for reuse in the construction sector, J. Clean. Prod. 122 (2016) 335–344, https://doi.org/10.1016/j.jclepro.2016.02.045.

[10] L.G. Li, A.K.H. Kwan, Adding limestone fines as cementitious paste replacement to improve tensile strength, stiffness and durability of concrete, Cem. Concr. Compos. 60 (2015) 17–24, https://doi.org/10.1016/j.cemconcomp.2015.02.006.

[11] N. Ghafoori, R. Spitek, M. Najimi, Influence of limestone size and content on transport properties of self-consolidating concrete, Constr. Build. Mater. 127 (2016) 588–595, https://doi.org/10.1016/j.conbuildmat.2016.10.051.
[12] G. İnan Sezer, Compressive strength and sulfate resistance of limestone and/or silica fume mortars, Constr. Build. Mater. 26 (2012) 613–618, https://doi.org/10.1016/j.conbuildmat.2011.06.064.
[13] C. Li, L. Jiang, N. Xu, S. Jiang, Pore structure and permeability of concrete with high volume of limestone powder addition, Powder Technol. 338 (2018) 416–424, https://doi.org/10.1016/j.powtec.2018.07.054.
[14] A.M. Diab, A.E.M. Abd Elmoaty, A.A. Aly, Long term study of mechanical properties, durability and environmental impact of limestone cement concrete, Alex. Eng. J. 55 (2016) 1465–1482, https://doi.org/10.1016/j.aej.2016.01.031.
[15] I.Y. Hakeem, M. Amin, I.S. Agwa, M.H. Abd-Elrahman, M.F. Abdelmagied, Using a combination of industrial and agricultural wastes to manufacture sustainable ultra-high-performance concrete, Case Stud. Constr. Mater. 19 (2023) e02323, https://doi.org/10.1016/j.cscm.2023.e02323.
[16] I.Y. Hakeem, M. Amin, I.S. Agwa, M.S. Rizk, M.F. Abdelmagied, Effect of using sugarcane leaf ash and granite dust as partial replacements for cement on characteristics of ultra-high performance concrete, Case Stud. Constr. Mater. 19 (2023) e02266, https://doi.org/10.1016/j.cscm.2023.e02266.
[17] S.H.P.W.C. Kosmatka , Design and control of concrete mixtures, Portland Cement Association, Skokie, IL, 2002.
[18] M.A. DeRousseau, E. Laftchiev, J.R. Kasprzyk, B. Rajagopalan, W.V. Srubar, A comparison of machine learning methods for predicting the compressive strength of field-placed concrete, Constr. Build. Mater. 228 (2019) 116661, https://doi.org/10.1016/j.conbuildmat.2019.08.042.
[19] T. Ji, T. Lin, X. Lin, A concrete mix proportion design algorithm based on artificial neural networks, Cem. Concr. Res. 36 (2006) 1399–1408, https://doi.org/10.1016/j.cemconres.2006.01.009.
[20] M.-Y. Cheng, P.M. Firdausi, D. Prayogo, High-performance concrete compressive strength prediction using Genetic Weighted Pyramid Operation Tree (GWPOT, Eng. Appl. Artif. Intell. 29 (2014) 104–113, https://doi.org/10.1016/j.engappai.2013.11.014.
[21] S. Popovics, J. Ujhelyi, Contribution to the Concrete Strength versus Water-Cement Ratio Relationship, J. Mater. Civ. Eng. 20 (2008) 459–463, https://doi.org/10.1061/(ASCE)0899-1561(2008)20:7(459).
[22] J. Namyong, Y. Sangchun, C. Hongbum, Prediction of Compressive Strength of In-Situ Concrete Based on Mixture Proportions, J. Asian Archit. Build. Eng. 3 (2004) 9–16, https://doi.org/10.3130/jaabe.3.9.
[23] K.A. Soudki, E.F. El-Salakawy, N.B. Elkum, Full Factorial Optimization of Concrete Mix Design for Hot Climates, J. Mater. Civ. Eng. 13 (2001) 427–433, https://doi.org/10.1061/(ASCE)0899-1561(2001)13:6(427).
[24] B. Bharatkumar, R. Narayanan, B. Raghuprasad, D. Ramachandramurthy, Mix proportioning of high performance concrete, Cem. Concr. Compos. 23 (2001) 71–80, https://doi.org/10.1016/S0958-9465(00)00071-8.
[25] M.F.M. Zain, S.M. Abd, Multiple Regression Model for Compressive Strength Prediction of High Performance Concrete, J. Appl. Sci. 9 (2008) 155–160, https://doi.org/10.3923/jas.2009.155.160.
[26] H.-B. Ly, T.-A. Nguyen, H.-V. Thi Mai, V.Q. Tran, Development of deep neural network model to predict the compressive strength of rubber concrete, Constr. Build. Mater. 301 (2021) 124081, https://doi.org/10.1016/j.conbuildmat.2021.124081.
[27] F.H. Chiew, C.K. Ng, K.C. Chai, K.M. Tay, A Fuzzy Adaptive Resonance Theory-Based Model for Mix Proportion Estimation of High-Performance Concrete, Comput. -Aided Civ. Infrastruct. Eng. 32 (2017) 772–786, https://doi.org/10.1111/mice.12288.
[28] B.A. Salami, T. Olayiwola, T.A. Oyehan, I.A. Raji, Data-driven model for ternary-blend concrete compressive strength prediction using machine learning approach, Constr. Build. Mater. 301 (2021) 124152, https://doi.org/10.1016/j.conbuildmat.2021.124152.
[29] S.A. Bello, L. Oyedele, O.K. Olaitan, K.A. Olonade, A.M. Olajumoke, A. Ajayi, L. Akanbi, O. Akinade, M.L. Sanni, A.-L. Bello, A deep learning approach to concrete water-cement ratio prediction, Results Mater. 15 (2022) 100300, https://doi.org/10.1016/j.rinma.2022.100300.
[30] J.-S. Chou, C.-K. Chiu, M. Farfoura, I. Al-Taharwa, Optimizing the Prediction Accuracy of Concrete Compressive Strength Based on a Comparison of Data-Mining Techniques, J. Comput. Civ. Eng. 25 (2011) 242–253, https://doi.org/10.1061/(ASCE)CP.1943-5487.0000088.
[31] A. Ahmad, V. Plevris, Q.-Z. Khan, Prediction of Properties of FRP-Confined Concrete Cylinders Based on Artificial Neural Networks, Crystals 10 (2020) 811, https://doi.org/10.3390/cryst10090811.
[32] Q. Ren, M. Li, M. Zhang, Y. Shen, W. Si, Prediction of Ultimate Axial Capacity of Square Concrete-Filled Steel Tubular Short Columns Using a Hybrid Intelligent Algorithm, Appl. Sci. 9 (2019) 2802, https://doi.org/10.3390/app9142802.
[33] A. Ahmad, W. Ahmad, F. Aslam, P. Joyklad, Compressive strength prediction of fly ash-based geopolymer concrete via advanced machine learning techniques, Case Stud. Constr. Mater. 16 (2022) e00840, https://doi.org/10.1016/j.cscm.2021.e00840.
[34] D. Dao, H.-B. Ly, S. Trinh, T.-T. Le, B. Pham, Artificial Intelligence Approaches for Prediction of Compressive Strength of Geopolymer Concrete, Materials 12 (2019) 983, https://doi.org/10.3390/ma12060983.
[35] S.R. Vadyala, S.N. Betgeri, J.C. Matthews, E. Matthews, A review of physics-based machine learning in civil engineering, Results Eng. 13 (2022) 100316, https://doi.org/10.1016/J.RINENG.2021.100316.
[36] A.T. Huynh, Q.D. Nguyen, Q.L. Xuan, B. Magee, T. Chung, K.T. Tran, K.T. Nguyen, A Machine Learning-Assisted Numerical Predictor for Compressive Strength of Geopolymer Concrete Based on Experimental Data and Sensitivity Analysis, Appl. Sci. 10 (2020) 7726, https://doi.org/10.3390/app10217726.
[37] M. Mohtasham Moein, A. Saradar, K. Rahmati, S.H. Ghasemzadeh Mousavinejad, J. Bristow, V. Aramali, M. Karakouzian, Predictive models for concrete properties using machine learning and deep learning approaches: A review, J. Build. Eng. 63 (2023) 105444, https://doi.org/10.1016/j.jobe.2022.105444.
[38] P. Lu, S. Chen, Y. Zheng, Artificial Intelligence in Civil Engineering, Math. Probl. Eng. 2012 (2012) 1–22, https://doi.org/10.1155/2012/145974.
[39] B. Boukhatem, S. Kenai, A. Tagnit-Hamou, M. Ghrici, APPLICATION OF NEW INFORMATION TECHNOLOGY ON CONCRETE: AN OVERVIEW / NAUJŲ INFORMACINIŲ TECHNOLOGIJŲ NAUDOJIMAS RUOŠIANT BETONĄ. APŽVALGA, J. Civ. Eng. Manag. 17 (2011) 248–258, https://doi.org/10.3846/13923730.2011.574343.
[40] S. Nazar, J. Yang, A. Ahmad, S.F.A. Shah, Comparative study of evolutionary artificial intelligence approaches to predict the rheological properties of fresh concrete, Mater. Today Commun. 32 (2022) 103964, https://doi.org/10.1016/j.mtcomm.2022.103964.
[41] H. Song, A. Ahmad, F. Farooq, K.A. Ostrowski, M. Maślak, S. Czarnecki, F. Aslam, Predicting the compressive strength of concrete with fly ash admixture using machine learning algorithms, Constr. Build. Mater. 308 (2021) 125021, https://doi.org/10.1016/j.conbuildmat.2021.125021.
[42] Q. Wang, A. Hussain, M.U. Farooqi, A.F. Deifalla, Artificial intelligence-based estimation of ultra-high-strength concrete's flexural property, Case Stud. Constr. Mater. 17 (2022) e01243, https://doi.org/10.1016/j.cscm.2022.e01243.
[43] H.U. Ahmed, A.S. Mohammed, R.H. Faraj, A.A. Abdalla, S.M.A. Qaidi, N.H. Sor, A. A. Mohammed, Innovative modeling techniques including MEP, ANN and FQ to forecast the compressive strength of geopolymer concrete modified with nanoparticles, Neural Comput. Appl. 35 (2023) 12453–12479, https://doi.org/10.1007/s00521-023-08378-3.
[44] M.-Y. Cheng, J.-S. Chou, A.F.V. Roy, Y.-W. Wu, High-performance Concrete Compressive Strength Prediction using Time-Weighted Evolutionary Fuzzy Support Vector Machines Inference Model, Autom. Constr. 28 (2012) 106–115, https://doi.org/10.1016/j.autcon.2012.07.004.
[45] A.F. Kocamaz, Y. Ayaz, M.B. Karakoç, İ. Türkmen, R. Demirboğa, Prediction of compressive strength and ultrasonic pulse velocity of admixtured concrete using tree model M5P, Struct. Concr. 22 (2021), https://doi.org/10.1002/suco.202000061.
[46] Q. Han, C. Gui, J. Xu, G. Lacidogna, A generalized method to predict the compressive strength of high-performance concrete by improved random forest algorithm, Constr. Build. Mater. 226 (2019) 734–742, https://doi.org/10.1016/j.conbuildmat.2019.07.315.
[47] J.-H. Choi, D. Kim, M.-S. Ko, D.-E. Lee, K. Wi, H.-S. Lee, Compressive strength prediction of ternary-blended concrete using deep neural network with tuned hyperparameters, J. Build. Eng. 75 (2023) 107004, https://doi.org/10.1016/j.jobe.2023.107004.
[48] M. Haenlein, A. Kaplan, A Brief History of Artificial Intelligence: On the Past, Present, and Future of Artificial Intelligence, Calif. Manag. Rev. 61 (2019) 5–14, https://doi.org/10.1177/0008125619864925.
[49] O. Avci, O. Abdeljaber, S. Kiranyaz, M. Hussein, M. Gabbouj, D.J. Inman, A review of vibration-based damage detection in civil structures: From traditional methods to Machine Learning and Deep Learning applications, Mech. Syst. Signal Process. 147 (2021) 107077, https://doi.org/10.1016/j.ymssp.2020.107077.
[50] Y. Bengio, Learning Deep Architectures for AI, Found. Trends® Mach. Learn. 2 (2009) 1–127, https://doi.org/10.1561/2200000006.
[51] J. Schmidhuber, Deep learning in neural networks: An overview, Neural Netw. 61 (2015) 85–117, https://doi.org/10.1016/j.neunet.2014.09.003.
[52] T.G. Dietterich, Ensemble Methods in, Mach. Learn., (2000) 1–15, https://doi.org/10.1007/3-540-45014-9_1.
[53] S. Oyebisi, T. Alomayri, Artificial intelligence-based prediction of strengths of slag-ash-based geopolymer concrete using deep neural networks, Constr. Build. Mater. 400 (2023) 132606, https://doi.org/10.1016/j.conbuildmat.2023.132606.
[54] P. Chopra, R.K. Sharma, M. Kumar, T. Chopra, Comparison of Machine Learning Techniques for the Prediction of Compressive Strength of Concrete, Adv. Civ. Eng. 2018 (2018) 1–9, https://doi.org/10.1155/2018/5481705.
[55] J. Abellán-García, Four-layer perceptron approach for strength prediction of UHPC, Constr. Build. Mater. 256 (2020) 119465, https://doi.org/10.1016/j.conbuildmat.2020.119465.
[56] C. Yang, H. Feng, M. Esmaeili-Falak, *Retracted:* Predicting the compressive strength of modified recycled aggregate concrete, Struct. Concr. 23 (2022) 3696–3717, https://doi.org/10.1002/suco.202100681.
[57] B.A. Young, A. Hall, L. Pilon, P. Gupta, G. Sant, Can the compressive strength of concrete be estimated from knowledge of the mixture proportions?: New insights from statistical analysis and machine learning methods, Cem. Concr. Res. 115 (2019) 379–388, https://doi.org/10.1016/j.cemconres.2018.09.006.
[58] N. Chen, S. Zhao, Z. Gao, D. Wang, P. Liu, M. Oeser, Y. Hou, L. Wang, Virtual mix design: Prediction of compressive strength of concrete with industrial wastes using deep data augmentation, Constr. Build. Mater. 323 (2022) 126580, https://doi.org/10.1016/j.conbuildmat.2022.126580.
[59] I. Ranjbar, V. Toufigh, M. Boroushaki, A combination of deep learning and genetic algorithm for predicting the compressive strength of <scp>high-performance</scp> concrete, Struct. Concr. 23 (2022) 2405–2418, https://doi.org/10.1002/suco.202100199.
[60] BS EN 197-1, Cement - Composition, specifications and conformity criteria for common cements, London, 2019.
[61] BS EN 12620, Aggregates for concrete, 2013.
[62] BS EN 196-3, Method of Testing Cement: Physical Test, London, 2016.

[63] ASTM C 618-19, Standard Specification for Fly Ash and Raw or Calcined Natural Pozzolan for Use as a Mineral Admixture, West Conshohocken, PA, 2022.
[64] American Concrete Institute 211-1, Standard Practice for Selecting Proportions for Normal, Heavyweight, and Mass Concrete, USA, 2002.
[65] B.A. Tayeh, M.W. Hasaniyah, A.M. Zeyad, M.O. Yusuf, Properties of concrete containing recycled seashells as cement partial replacement: A review, J. Clean. Prod. 237 (2019) 117723, https://doi.org/10.1016/j.jclepro.2019.117723.
[66] British Standard EN 12390- 4, Testing Hardened Concrete: Compressive Strength of Test Specimens, London, 2019.
[67] British Standard EN 12390-1, Testing Hardened Concrete: Making and Curing for Strength Test, London, 2019.
[68] British Standard EN 12390-5, Testing Hardened Concrete: Flexural Strength of Test Specimens, London, 2019.
[69] British Standard EN 12390-6, Testing Hardened Concrete: Splitting Tensile Strength of Test Specimens, London, 2019.
[70] H.B.D.M.H.B.O.D.J. Martin T. Hagan, Neural Network Design, 2nd ed., Martin Hagan, Oklahoma, 2014.
[71] G. Panchal, A. Ganatra, Y.P. Kosta, D. Panchal, Behaviour Analysis of Multilayer Perceptronswith Multiple Hidden Neurons and Hidden Layers, Int. J. Comput. Theory Eng. (2011) 332–337, https://doi.org/10.7763/IJCTE.2011.V3.328.
[72] M. Uzair, N. Jamil, Effects of Hidden Layers on the Efficiency of Neural networks, in: 2020 IEEE 23rd International Multitopic Conference (INMIC), IEEE, 2020: pp. 1–6. https://doi.org/10.1109/INMIC50486.2020.9318195.
[73] S. Oyebisi, H. Owamah, M. Omeje, Application of machine learning algorithm in the internal and external hazards from industrial byproducts, Clean. Eng. Technol. 13 (2023) 100629, https://doi.org/10.1016/j.clet.2023.100629.
[74] S. Oyebisi, T. Igba, F. Olutoge, A. Ede, Application of artificial intelligence in the hazard indexes of recycled agricultural waste materials, Multiscale Multidiscip. Model., Exp. Des. (2023), https://doi.org/10.1007/s41939-023-00327-w.
[75] A. Raheem, B. Ikotun, S. Oyebisi, A. Ede, Machine learning algorithms in wood ash-cement-Nano TiO2-based mortar subjected to elevated temperatures, Results Eng. 18 (2023) 101077, https://doi.org/10.1016/j.rineng.2023.101077.
[76] B.N. Ekwueme, Deep neural network modeling of river discharge in a tropical humid watershed, Earth Sci. Inform. (2024), https://doi.org/10.1007/s12145-023-01219-w.
[77] S.A. Alabi, C. Arum, A.P. Adewuyi, R.C. Arum, J.O. Afolayan, J. Mahachi, Mathematical model for prediction of compressive strength of ternary blended cement concrete utilizing gene expression programming, Sci. Afr. 22 (2023) e01954, https://doi.org/10.1016/j.sciaf.2023.e01954.
[78] A. Sivasubramanian, S. Arathy Krishna, D.H. Nair, K. Varma, R. Radhakrishnan, D. Sathyan, Experimental validation of compressive strength prediction using machine learning algorithm, Mater. Today.: Proc. 64 (2022) 181–187, https://doi.org/10.1016/j.matpr.2022.04.362.
[79] F. Farooq, M. Nasir Amin, K. Khan, M. Rehan Sadiq, M.F. Faisal Javed, F. Aslam, R. Alyousef, A Comparative Study of Random Forest and Genetic Engineering Programming for the Prediction of Compressive Strength of High Strength Concrete (HSC, Appl. Sci. 10 (2020) 7330, https://doi.org/10.3390/app10207330.
[80] D.M. Hamby, A review of techniques for parameter sensitivity analysis of environmental models, Environ. Monit. Assess. 32 (1994) 135–154, https://doi.org/10.1007/BF00547132.
[81] K. Khan, B.A. Salami, A. Jamal, M.N. Amin, M. Usman, M.A. Al-Faiad, A.M. Abu-Arab, M. Iqbal, Prediction Models for Estimating Compressive Strength of Concrete Made of Manufactured Sand Using Gene Expression Programming Model, Materials 15 (2022) 5823, https://doi.org/10.3390/ma15175823.
[82] W. Xun, C. Wu, X. Leng, J. Li, D. Xin, Y. Li, Effect of Functional Superplasticizers on Concrete Strength and Pore Structure, Appl. Sci. 10 (2020) 3496, https://doi.org/10.3390/app10103496.
[83] S. Kourounis, S. Tsivilis, P.E. Tsakiridis, G.D. Papadimitriou, Z. Tsibouki, Properties and hydration of blended cements with steelmaking slag, Cem. Concr. Res. 37 (2007) 815–822, https://doi.org/10.1016/j.cemconres.2007.03.008.
[84] J. Wang, E. Liu, L. Li, Characterization on the recycling of waste seashells with Portland cement towards sustainable cementitious materials, J. Clean. Prod. 220 (2019) 235–252, https://doi.org/10.1016/j.jclepro.2019.02.122.
[85] S.O. Oyebisi, A.N. Ede, F.A. Olutoge, Optimization of Design Parameters of Slag-Corncob Ash-Based Geopolymer Concrete by the Central Composite Design of the Response Surface Methodology, Iran. J. Sci. Technol. - Trans. Civ. Eng. 45 (2021), https://doi.org/10.1007/s40996-020-00470-1.
[86] S. Oyebisi, A. Ede, F. Olutoge, B. Ngene, Assessment of activity indexes on the splitting tensile strengthening of geopolymer concrete incorporating supplementary cementitious materials, Mater. Today Commun. 24 (2020), https://doi.org/10.1016/j.mtcomm.2020.101356.
[87] Abdullahi, Effect of aggregate type on Compressive strength of concrete, Int. J. Civ. Struct. Eng. 2 (2012), https://doi.org/10.6088/ijcser.00202030008.
[88] Y. Peng, C. Unluer, Analyzing the mechanical performance of fly ash-based geopolymer concrete with different machine learning techniques, Constr. Build. Mater. 316 (2022) 125785, https://doi.org/10.1016/J.CONBUILDMAT.2021.125785.
[89] A. Hassan, M. Arif, M. Shariq, Use of geopolymer concrete for a cleaner and sustainable environment – A review of mechanical properties and microstructure, J. Clean. Prod. 223 (2019) 704–728, https://doi.org/10.1016/j.jclepro.2019.03.051.
[90] H.-B. Le, Q.-B. Bui, L. Tang, Geopolymer Recycled Aggregate Concrete: From Experiments to Empirical Models, Materials 14 (2021) 1180, https://doi.org/10.3390/ma14051180.
[91] G.A.K.D.O. Kiambigi Maina, Effects of different fine aggregates on concrete strength, in: Proceedings of the Sustainable, Res. Innov. Conf., KUAT Main. Campus, Kenya (2018) 135–140.
[92] A.M. Neville. Properties of concrete, 4th ed., Longman, Harlow, U.K, 1995.
[93] X.-Y. Wang, Analysis of hydration and strength optimization of cement-fly ash-limestone ternary blended concrete, Constr. Build. Mater. 166 (2018) 130–140, https://doi.org/10.1016/j.conbuildmat.2018.01.058.
[94] A.N. Ede, O.M. Olofinnade, A.I. Akpabot, S.O. Oyebisi, D.O. Nduka, Influence of Dicalcium Silicate and Tricalcium Aluminate Compounds in Different Local Cement Brands on the Compressive Strength of Normal Concrete, 2021. https://doi.org/10.4028/www.scientific.net/SSP.318.59.
[95] W. Ahmad, A. Ahmad, K.A. Ostrowski, F. Aslam, P. Joyklad, P. Zajdel, Application of Advanced Machine Learning Approaches to Predict the Compressive Strength of Concrete Containing Supplementary Cementitious Materials, Materials 14 (2021) 5762, https://doi.org/10.3390/ma14195762.
[96] H. Naderpour, A.H. Rafiean, P. Fakharian, Compressive strength prediction of environmentally friendly concrete using artificial neural networks, J. Build. Eng. 16 (2018) 213–219, https://doi.org/10.1016/j.jobe.2018.01.007.
[97] I. Shafi, J. Ahmad, S.I. Shah, F.M. Kashif, Impact of Varying Neurons and Hidden Layers in Neural Network Architecture for a Time Frequency Application, in: 2006 IEEE International Multitopic Conference, IEEE, 2006: pp. 188–193. https://doi.org/10.1109/INMIC.2006.358160.
[98] Cort J. Willmott, Kenji Matsuura, Advantages of the mean absolute error (MAE) over the root mean square error (RMSE) in assessing average model performance, Clim. Res. 30 (2005) 79–82.